Journal of Human Evolution 153 (2021) 102956

Contents lists available at ScienceDirect

Journal of Human Evolution

journal homepage: www.elsevier.com/locate/jhevol

New Pliocene hominin remains from the Leado Dido'a area of Woranso-Mille, Ethiopia

Stephanie M. Melillo [a, *], Luis Gibert [b], Beverly Z. Saylor [c], Alan Deino [d], Mulugeta Alene [e], Timothy M. Ryan [f], Yohannes Haile-Selassie [g, h]

[a] Department of Human Evolution, Max Planck Institute for Evolutionary Anthropology Leipzig, Germany
[b] Departament de Mineralogia, Petrologia i Geologia Aplicada Facultat de Ciències de la Terra, Universitat de Barcelona, Barcelona, Spain
[c] Department of Earth, Environmental and Planetary Sciences, Case Western Reserve University, Cleveland, OH, USA
[d] Berkeley Geochronology Center, Berkeley, CA, USA
[e] School of Earth Sciences, Addis Ababa University, Addis Ababa, Ethiopia
[f] Department of Anthropology, Pennsylvania State University, University Park, PA, USA
[g] Department of Physical Anthropology, Cleveland Museum of Natural History, Cleveland, OH, USA
[h] Departments of Anthropology and Biology, Case Western Reserve University, Cleveland, OH, USA

ARTICLE INFO

Article history:
Received 3 September 2020
Accepted 25 January 2021
Available online 9 March 2021

Keywords:
Australopithecus afarensis
Variation
Taxonomic diversity
Sidi Hakoma Tuff
Maxilla
Mandible

ABSTRACT

Fossiliferous deposits at Woranso-Mille span the period when *Australopithecus anamensis* gave rise to *Australopithecus afarensis* (3.8–3.6 Ma) and encompass the core of the *A. afarensis* range (ca. 3.5–3.2 Ma). Within the latter period, fossils described to date include the intriguing but taxonomically unattributed Burtele foot, dentognathic fossils attributed to *Australopithecus deyiremeda*, and one specimen securely attributed to *A. afarensis* (the Nefuraytu mandible). These fossils suggest that at least one additional hominin lineage lived alongside *A. afarensis* in the Afar Depression. Here we describe a collection of hominin fossils from a new locality in the Leado Dido'a area of Woranso-Mille (LDD-VP-1). The strata in this area are correlated to the same chron as those in the Burtele area (C2An.3n; 3.59–3.33 Ma), and similar in age to the Maka Sands and the Basal through lower Sidi Hakoma Members of the Hadar Formation. We attribute all but one of the LDD hominin specimens to *A. afarensis*, based on diagnostic morphology of the mandible, maxilla, canines, and premolars. The LDD specimens generally fall within the range of variation previously documented for *A. afarensis* but increase the frequency of some rare morphological variants. However, one isolated M_3 is extremely small, and its taxonomic affinity is currently unknown. The new observations support previous work on temporal trends in *A. afarensis* and demonstrate that the large range of variation accepted for this species is present even within a limited spatiotemporal range. The value added with this sample lies in its contribution to controlling for spatiotemporal differences among site samples in the *A. afarensis* hypodigm and its contemporaneity with non-*A. afarensis* specimens at Woranso-Mille.

1. Introduction

Australopithecus afarensis is the best-known early hominin species from eastern Africa. At the time of its initial description, this species was the oldest and most primitive hominin identified and was accordingly considered ancestral to all later species (Johanson and White, 1979). Although our perspective has changed with the discovery of much older species, *A. afarensis* remains central to our understanding of early hominin paleobiology and systematics. This species strongly influences the way the australopith ecological niche is characterized and constitutes an important comparative reference for all early hominins. The history of research on *A. afarensis* has shaped current attitudes and approaches to recognizing species and lineages in the fossil record (Kimbel and Delezene, 2009; Kimbel, 2015).

Woranso-Mille (Afar, Ethiopia) is one of the more recently discovered paleontological sites preserving *A. afarensis* remains. Fossil collection localities at Woranso-Mille can be grouped into two distinct, but informal, chronostratigraphic packages. The Western Exposure Area (WEA) includes localities dated to

* Corresponding author.
E-mail address: stephanie_melillo@eva.mpg.de (S.M. Melillo).

https://doi.org/10.1016/j.jhevol.2021.102956
0047-2484/

3.8–3.57 Ma (Deino et al., 2010; Saylor et al., 2016, 2019). The WEA localities are characterized by fossiliferous sediments interbedded with a distinct sequence of marker tuffs that fill a temporal gap between the oldest fossils assigned to *A. afarensis* (Harrison, 2011; Johanson et al., 1978; White, 1977, 1980) and the youngest fossils of its presumed ancestor, *Australopithecus anamensis.* Hominin fossils from WEA localities have been assigned to *A. anamensis* (Haile-Selassie et al., 2019), to *A. afarensis* (Haile-Selassie et al., 2010a; Haile-Selassie and Ryan, 2019), or as representing transitional populations along an evolving *A. anamensis-A. afarensis* lineage (Haile-Selassie, 2010; Haile-Selassie et al., 2010b).

The Eastern Exposure Area (EEA; Fig. 1) includes localities ranging from >3.469 to <3.2 Ma (Haile-Selassie et al., 2015, 2016a), which approximates the temporal range covered by the sites that produced the core of the *A. afarensis* hypodigm (Hadar: Drapeau et al., 2005; Johanson et al., 1982a, b; Kimbel et al., 1982, 2004; Kimbel and Rak, 2010; White and Johanson, 1982; Dikika: Alemseged et al., 2005, 2006; Maka: Lovejoy et al., 2002; White et al., 1993, 2000). Hominin fossils from the EEA include the taxonomically unassigned Burtele foot (Haile-Selassie et al., 2012), dentognathic remains assigned to *Australopithecus deyiremeda* (also collected from localities in the Burtele area, see Haile-Selassie et al., 2015) and *A. afarensis* (Haile-Selassie et al., 2016a). The latter species is represented by the Nefuraytu mandible, which exhibits typical, diagnostic *A. afarensis* morphology. To date, the Nefuraytu mandible is the only specimen from an EEA locality assigned to *A. afarensis*. Here, we provide the comparative description and taxonomic assignment for a sample of hominin fossils collected from a new EEA locality located within the Leado Dido'a area of Woranso-Mille, LDD-VP-1.

Samples constituting the *A. afarensis* hypodigm are morphologically variable. This observation was made in the original species diagnosis (Johanson et al., 1978), and factors responsible for the large magnitude of variation have been investigated ever since. Commonly discussed contributing factors include sexual dimorphism (Plavcan et al., 2005; but see; Reno and Lovejoy, 2015; Reno et al., 2010), temporal trends (Lockwood et al., 2000; Kimbel et al., 2006; Delezene and Kimbel, 2011), and taxonomic heterogeneity. With regard to the latter factor, research efforts of the 1970–1980s focused on the number of species present in the Hadar or Laetoli + Hadar samples (Coppens, 1983; Kimbel et al., 1985; Olson, 1981, 1985; Sénut, 1983; Senut and Tardieu, 1985; White, 1985; also reviewed by Kimbel and Delezene, 2009), but general agreement was reached in the 1990s that these collections are taxonomically homogeneous.

Since that time, additional middle Pliocene hominin fossils have been discovered that fall outside the already large range of variation accepted for *A. afarensis* (i.e., *Kenyanthropus platyops* and other specimens from Lomekwi, West Turkana, Kenya: Brown et al., 2001; Delezene and Kimbel, 2011; Leakey et al., 2001; Skinner et al., 2020; Spoor et al., 2016; *Australopithecus bahrelghazali*: Brunet et al., 1996; Guy et al., 2008; the Burtele foot: Haile-Selassie et al., 2012; and *A. deyiremeda*: Haile-Selassie et al., 2015; Spoor et al., 2016). The topic of middle Pliocene taxonomic diversity is garnering increasing attention based on these newly discovered fossils. While a range of opinions exist, recent reviews categorize the evidence for the taxonomic distinctness of *K. platyops* as moderate (Wood and Boyle, 2016) or strong (Kimbel, 2015), and the Burtele foot has been described as the most convincing evidence of middle Pliocene lineage diversity currently known (Kimbel, 2015; Klein, 2016; Wood and Boyle, 2016; Haile-Selassie et al., 2016b).

Still, additional evidence is needed to further evaluate the hypothesis of middle Pliocene taxonomic diversity. Sample sizes of proposed non-*A. afarensis* species are small (often $n = 1$ or 2), and many of these fossils are fragmentary or poorly preserved, with spotty anatomical coverage. These challenges restrict the thoroughness with which morphological differences between *A. afarensis* and potential non-*A. afarensis* species can be characterized.

Furthermore, spatiotemporal discontinuities among previously known site samples and small sample limitations create viable alternatives to the taxonomic diversity hypothesis—namely, that morphological differences between *A. afarensis* and other proposed middle Pliocene species are attributable to temporal or geographic variation, stochastic population-level differences, or sampling error of a single species. These variation-inflating factors are confounded in most comparisons across site samples, so it is difficult to disentangle the effects of differences in time and space from stochastic differences among populations or samples.

New site samples that increase sample size and fill existing spatiotemporal gaps permit more controlled comparisons that address these issues. The EEA deposits at Woranso-Mille have minimal temporal and geographic distance from the core sample of the *A. afarensis* hypodigm, which makes these fossils well suited to investigating if and how middle Pliocene hominins at Woranso-Mille differ from *A. afarensis* at Hadar, Dikika, and Maka.

The fossiliferous deposits at LDD-VP-1 have been surveyed annually since their discovery in 2007. Over 1300 vertebrate fossils have been recovered to date, including multiple hominins (Table 1). This locality lies 3.5 km southeast of the Burtele area and 5 km southwest of Nefuraytu (Fig. 1A). The close proximity of LDD-VP-1 to the Burtele area raises the possibility that the sample could contain additional remains of the non-*A. afarensis* species represented there. The LDD collection includes maxillae and mandibles that preserve most of the morphological features used to diagnose *A. afarensis* and non-*A. afarensis* middle Pliocene hominins. This study presents anatomical and comparative descriptions of the LDD hominin fossils and provides their chronostratigraphic context. We focus on the taxonomic attribution of the hominins and further investigate evidence of taxonomic diversity in the Woranso-Mille EEA sample.

2. Materials and methods

2.1. Tephrochemistry

We analyzed the tephrochemistry of ash samples collected at three locations in the Leado Dido'a area (described in Section 3.1 Stratigraphy). Elemental abundances of volcanic glass were analyzed in polished grain mounts using a Cameca SX-51 electron probe micro-analyzer at the University of Wisconsin, Madison, following the methods in Saylor et al. (2016). The mounts were carbon coated at the same time as standards, which included Kilbourne Olivine for Mg, Minas Gerais rutile for Ti, Monash andesine for Ca, synthetic manganese olivine for Mn, Rockport fayalite for Fe, Topaz for F, USMN chlorapatite for Cl, and Lipari Obsidian for Si, Al, O, Na, and K. Analyses were conducted using a focused beam, an accelerating voltage of 15 KeV, a beam current of 10 nA, with on-peak and off-peak count times of 20 s. Na, K, O, and Si were corrected for ion migration using time-dependent intensity data, and elemental concentrations were converted to oxides, computing all Fe and Fe_2O_3. Average oxide concentrations were normalized to H_2O^*-free totals to account for differences in water content of the glass, in which water content (H_2O^*) is measured O minus halogen-corrected stoichiometric O.

2.2. Paleomagnetism

Fifteen paleomagnetic samples were collected in stratigraphic sequence in the Leado Dido'a area. Fine-grained strata (claystone,

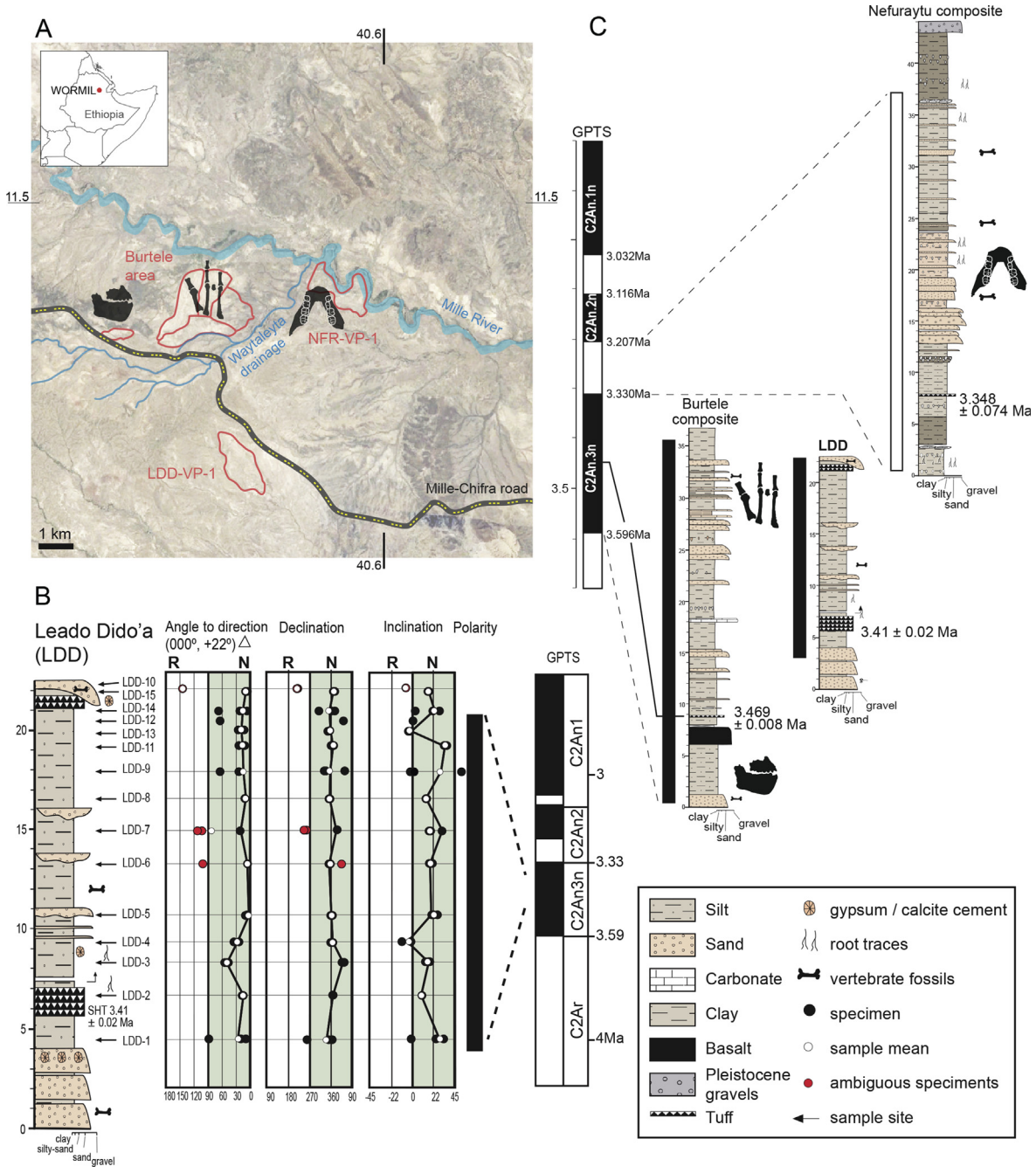

Figure 1. LDD-VP-1 geography and geological context. (A) Map showing location of LDD-VP-1 in relation to other EEA collection areas at Nefuraytu (NFR-VP-1) and Burtele (BRT-VP-1, -2, -3 and WYT-VP-1, -2). (B) Magnetostratigraphy for the LDD-VP-1 section. The stratigraphic position of studied samples is shown, with values for primary directions (declination/inclination). Sample polarity is expressed as delta (angle to the expected Normal direction 000/+22). All samples exhibit normal polarity, except for the uppermost (LDD-10), which show an ambiguous direction interpreted as a remagnetization following a lightning strike. The figure shows a correlation between the local LDD Normal polarity and the GPTS, aligned according to the previously reported age of SHT tuff. Red dots indicate specimens with mixed directions, black dots are useful specimen directions and white dots are mean sample values. (C) Stratigraphic section for LDD-VP-1, correlated to Burtele and Nefuraytu composite sections. (For interpretation of the references to color in this figure legend, the reader is referred to the Web version of this article.)

siltstone and fine sandstone) were preferentially sampled, in addition to one ash sample. After removing weathered material, sample blocks of ca. 500 cm^3 were cut from outcrops and oriented using a Brunton compass. Each sample was sawn, sanded, and cleaned with compressed air in the laboratory to obtain between one and three cubic specimens (8 cm^3) for measurement. Measurements were performed at the Laboratory of Paleomagnetism in the Institute of Earth Sciences Jaume Almera (Barcelona). The Natural Remanent Magnetisation was measured on a DC SQUID superconducting rock magnetometer (2G Enterprises Ltd, Sand City, CA). Thermal demagnetization was used to remove secondary magnetizations and isolate the primary magnetic polarity. Specimens were heated in stepwise thermal increments of 50 °C in a non-inductive furnace (<10nT) until 550 °C. Magnetic susceptibility was measured with a KLY-2 susceptibility bridge (Agico, Brno) at each demagnetization step, to monitor mineralogical changes during thermal demagnetization.

Table 1
Hominin fossils collected at LDD-VP-1.

Specimen number	Element	Year collected	Discovered by
LDD-VP-1/104	Tooth fragment	2007	Ali Idris
LDD-VP-1/126[a]	Maxilla (RI^1–C^1 roots, RP^3–P^4 and RM^2 crowns, LI^1–P^4 roots)	2007	Ali Idris
LDD-VP-1/131	Edentulous partial mandible; LM_3 fragment; cranial fragments ($n = 3$)	2007	Alemayehu Asfaw
LDD-VP-1/167[a]	Right mandible fragment (I_1–P_4 roots, M_1 crown)	2007	Ali Idris
LDD-VP-1/248	Right maxilla (I^1–P^3 alveoli, P^4–M^2 roots); Left maxilla fragment (I^1 alveolus and I^2 root); detached RI^1–P^4, LC^1 and tooth fragments	2008	Abush Kassu
LDD-VP-1/406	RM_3	2009	Kampiro Kayranto
LDD-VP-1/672	Mandibular corpus fragments and detached LC_1–M_2 crowns	2010	Burhan Nori
LDD-VP-1/732	LM_3	2011	Barao Mohammed
LDD-VP-1/764	RM_x fragment	2012	Kampiro Kayranto
LDD-VP-1/775	$LM^{1\ or 2}$ (worn)	2012	Mohammed Barao
LDD-VP-1/876	RM_x fragment	2014	Ahmed Elema
LDD-VP-1/1065	LM_3	2017	Tilahun Birile
LDD-VP-1/1111	tooth fragment	2017	Group

[a] Specimens could represent the same individual.

Samples showed high magnetic susceptibility at room temperature, and no major changes were recorded during the demagnetization steps. Overall, the samples yielded unblocking temperatures of <600 °C, indicating magnetite as the main carrier of magnetization. Paleomagnetic directions were calculated by means of principal component analysis (Kirschvink, 1980) using the Paldir software v. 5.5 (Utrecht University).

2.3. Morphological description and comparison

Anatomical terminology and metric definitions follow previous work on early hominins, particularly *A. afarensis* (White, 1977; White and Johanson, 1982; Kimbel et al., 1982, 2004; Johanson et al., 1982b; Suwa, 1990; Suwa et al., 1994; Ward et al., 2001, 2013, 2020; Spoor et al., 2010; Delezene and Kimbel, 2011). Characterization of premolar root configuration follows Moore et al. (2016). Metrics for the comparative fossil sample were compiled from the literature (White, 1977, 1980; Suwa, 1990; Suwa et al., 1994; Brunet et al., 1995, 1996; Leakey et al., 1995, 2001; Ward et al., 1999, 2001, 2013, 2020; White et al., 2000, 2006; Brown et al., 2001; Kimbel et al., 2004; Alemseged et al., 2005; Moggi-Cecchi et al., 2006; Spoor et al., 2010; Delezene and Kimbel, 2011; Harrison, 2011; Manthi et al., 2012; Haile-Selassie and Melillo, 2015; Haile-Selassie et al., 2015, 2016a, 2019; Mbua et al., 2016; Skinner et al., 2020) and checked for interobserver comparability in the course of the authors' first-hand study of the original specimens. For most morphological features, the LDD sample is too small to merit formal statistical tests. We report LDD values in relation to summary statistics (means and measures of variation) available for comparative samples.

Taxonomic affinity was assessed based on the expression of morphology in the LDD sample that has been used to differentiate early and middle Pliocene hominin species (White, 1977, 1980; Johanson et al., 1978; White et al., 1983; Leakey et al., 1995, 2001; Brunet et al., 1996; Ward et al., 2001, 2013, 2020; Kimbel et al., 2004; Guy et al., 2008; Kimbel and Delezene, 2009; Delezene and Kimbel, 2011; Manthi et al., 2012; Haile-Selassie et al., 2015; Spoor et al., 2016).

2.4. Fossil scanning and reconstruction

We created three-dimensional scans for select specimens in the LDD and comparative samples. The Center for Quantitative Imaging of Pennsylvania State University produced computed tomography (CT) scans of Woranso-Mille fossils, using a high-resolution scanner (OMNI-X HD600). Scan settings varied among specimens depending on size and preservation. Source energy settings were at either 180 kV and 250 μA or 180 kV and 150 μA, and voxel size ranged between 20 and 70 μm. We also collected surface scans with an Artec Spider structured light scanner, processed in Artec Studio 12 Professional software v. 12.1.6 (Artec3D, Luxembourg). Further manipulation and analysis of scans (including CT scan segmentation, reconstruction and measurement) was conducted in Avizo software v. 9.3.0 (Thermo Fisher Scientific, Waltham, MA).

We standardized maxilla and mandible orientation such that the alveolar and midline planes were orthogonal. For the maxilla, the alveolar plane was defined as paralleling the internal alveolar margin between the left and right premolars and right M^1. We chose these orientation points because they are preserved on LDD-VP-1/126 and many comparative specimens. For the mandible, the alveolar plane was defined as paralleling the alveolar margin between the left and right P_4–M_1.

Securely oriented specimens were used as references to orient more fragmentary specimens. To do so, we first identified homologous landmarks preserved in common on the unoriented target and oriented reference specimens. Landmarks were positioned around the dental arcade, at junctions between the alveolar margin and interdental septa. The specific landmark locations depended on the preservation state unique to each target-reference pair. Next, centroid size was calculated for the target and reference landmark configurations and the reference was scaled to the size of the target. Lastly, the target specimen was registered to the scaled reference, in its oriented space. In this way, the target specimen is brought into a standardized orientation by combining preserved anatomy with observations from better-preserved *Australopithecus* fossils.

For maxillae and mandibles preserving midline landmarks, scans were simply mirror-imaged to reconstruct missing regions. We also estimated arcade shape in one mandible that does not preserve the midline (LDD-VP-1/167). This specimen was oriented as describe above, taking care to choose a reference specimen with a similar curve to the dental arcade. The LDD-VP-1/167 mesh was then mirror-imaged, and the space between the non-adjoining halves was determined by estimating the width of the interdental septum between the right (preserved) and left (mirrored) central incisor roots.

Contours of the mandibular symphysis and corpus were examined in cross section. We sectioned digital meshes in a manner that emulates the traditional approach (White et al., 2000). Mandible sectioning planes were orthogonal to the alveolar plane and ran parallel through interproximal contact facets (IPCFs) or interdental septa. Maxillary palate depth was also measured in cross section. The palate depth sectioning plane was orthogonal to the alveolar plane and ran parallel through the left and right M^1/M^2 IPCFs (approximating a coronal plane section).

3. Results

3.1. Geology and geochronology results

Stratigraphy A 22-meter-thick stratigraphic section was measured at LDD-VP-1 between 11.4213°N, 40.5639°E (base) and 11.4264°N, 40.5621°E (top) in the Leado Dido'a area. The fossil-bearing sandstone is positioned at the 12 m level with silty clay horizons, rich in root casts, above and below it. The entire section generally consists of alternating siltstones and sandstones and includes two tuff beds (Fig. 1B). The lower of these is a ~1.5 m thick white vitric ash. Its upper 1.1 m shows sedimentary structures (cross-bedding) indicating fluvial reworking. The second tuff occurs near the top of the section, below a persistent sandstone horizon. This tuff has a distinctive yellow color and is about 0.4 m thick. The lower-most strata correspond to 4 m of fluvial sandstones cemented with gypsum and calcite, bearing vertebrate fossils. Above these deposits, deltaic foresets, with clinoforms of <1m were identified. These facies show paleoflows toward the NE-E. The lower vitric ash is not exposed toward the SW and its relations with the deltaic facies have not been observed.

We interpret the relationship between the deltaic deposits and sediments to the NE as a lateral change, from a small delta to a shallow pond with the vitric ash filling this pond. This shallow pond was <1.5 m deep (based on size of clinoforms) and >0.35 Km^2 (based on the local distribution of the lower tuff). The pond was filled with sediments after the deposition of the vitric ash and sedimentation continued in the area, with fluvial silts and sands affected by edaphic processes. Near the top of the section, the second tuff bed (40 cm thick) is overlaid by a sandstone unit cemented with gypsum that also contains fossils.

Tephrochemistry The lower vitric ash is exposed continuously over ~1 km along a drainage at the southern border of the fossil collection locality. There are additional, patchy exposures of the ash to the northwest, over a distance of ~1.8 km. The ash was sampled for tephrochemistry at three locations. Two samples, LDD-08-2 (11.4212°N, 40.5633°E) and ADY-09-1 (11.4186°N, 40.5703°E), were collected from the continuous exposures along the drainage to the south and southeast of the main LDD-VP-1 collection horizon, respectively. A third sample, LDD 13-4 (11.4369°N, 40.5563°E), was collected from isolated outcrops ca. 1.6 km northwest of the main collection area. Tephrochemistry results are reported in Table 2.

Based on chemical, physical, and stratigraphic similarities, the vitric ash deposits at LDD are correlated to the Sidi Hakoma Tuff (SHT), a distal tephra unit that is widely recognized in the southern Afar, including at Woranso-Mille. The SHT chemically correlates with the Tulu Bor Tuff of the Turkana Basin (Brown, 1982), which extends from Kenya to the Gulf of Aden (Sarna-Wojcicki et al., 1985; WoldeGabriel et al., 2013; Saylor et al., 2016). Vitroclasts of the LDD tuff feature the higher Al_2O_3 (>12.5 wt. %), lower Fe_2O_3 (~1.6 wt. %), and lower CaO (~0.32 wt. %) abundances that distinguish the SHT from other tephra deposits at Woranso-Mille (Saylor et al., 2016). This composition also characterizes other known SHT occurrences at Woranso-Mille. The ash deposits at LDD-VP-1 exhibit further similarities with SHT: the ash deposits are crystal-poor to aphyric and internal stratification ranges from massive to laminated. Given the shallow eastward dip in the area, the LDD deposits, which are ca. 3–6 km southeast of the Burtele area, are projected to lie stratigraphically above the Kerare-Burtele basalts, similar to exposures of the SHT at BDB-VP-1, ~10 km west-northwest of LDD-VP-1 (Saylor et al., 2016; Alene et al., 2017). As described below, the magnetic polarity of the tuff is also the same as the SHT. $^{40}Ar/^{39}Ar$ ages for the SHT and its correlates range from 3.45 to 3.42 Ma, with the older ages considered as maximums (Walter and Aronson, 1993; Campisano and Feibel, 2008; WoldeGabriel et al., 2013; Saylor et al., 2016). A correlate of the tuff in the Gulf of Aden has an orbitally tuned age of 3.41 Ma (β-Tulu Bor, deMenocal and Brown, 1999), consistent with the younger range of $^{40}Ar/^{39}Ar$ ages, which we consider a best estimate.

Paleomagnetism Paleomagnetism results are summarized in Figure 1B, and Supplementary Online Material (SOM) Table S1 and Figure S1. Seven samples revealed an unambiguous characteristic direction, with all three specimens from each station showing consistent normal direction (Class A) and a small (<30°) delta value. Four samples showed one or two specimens where the secondary magnetization was incompletely removed (Class B), resulting in ambiguous directions. Nevertheless, these four samples yielded at least one specimen showing a normal direction with declination toward the north hemisphere and positive inclinations. One sample (LDD-12) yielded only a single specimen, which showed an ambiguous shallow direction toward the N/NE of 65º/1º with a delta value of 66º.

The uppermost sample LDD-10 shows a mean direction 212º/-8º with delta 146º, suggesting reverse polarity. A close evaluation of the specimen directions from sample LDD-10 shows significant differences in respect to the rest of the sample collection. The intensity of the magnetization is two orders of magnitude higher in LDD-10 than in other samples (SOM Figs. S1, S2). Further, demagnetization plots show a single strong component in one specimen, while the others show the secondary component removed only at 100 °C. In the rest of the samples, the secondary component is removed at 250 °C. In addition, the three specimens from LDD-10 show small dispersion, with an a_{95} of only 2.8°. These particularities suggest that the remanence direction of this sample was reset by the large, but transient magnetic fields associated with in-ground currents from a lightning strike. Additional samples were collected from the same strata as the ambiguous samples LDD-10 and LDD-12, but 150m to the NW. Results from these additional samples (LDD-14 and LDD-15) confirm normal polarity for the complete LDD section.

The normal polarity interval identified at LDD-VP-1 can be assigned to chron C2An.3n, based on the previously reported ages of SHT tuff near the bottom of the section. This normal zone can be correlated with the nearby section at Burtele where this chron has been identified based on a $^{40}Ar/^{39}Ar$-dated local tuff (Haile-Selassie et al., 2015).

Chronology among site samples The combination of tuff geochemistry and paleomagnetism constrain the age of the LDD sample to 3.41–3.33 Ma, permitting precise chronostratigraphic placement relative to other hominin site samples. At Woranso-Mille, LDD-VP-1 falls within the age range of localities in the Burtele area, but older than NFR-VP-1 (Fig. 1C). Specimens recovered from Burtele span two time intervals: 3.596–3.469 Ma (BRT-VP-3) and 3.469–3.33 Ma (BRT-VP-1, 2 and WYT-VP-2; Haile-Selassie et al., 2015). The *A. deyiremeda* holotype maxilla (BRT-VP-3/1) and paratype mandible (BRT-VP-3/14) were recovered from sedimentary strata underlying a 3.469 ± 0.008 Ma tuff, and thus are slightly

Table 2
LDD-VP-1 tephrochemistry. Oxide abundances for the lower vitric ash at LDD-VP-1 and the surrounding region.

Oxide	LDD-08-2 ($n = 10$)	LDD 13-4 ($n = 4$)	ADY-09-1 ($n = 18$)	BDB-09-1[a] ($n = 12$)	ESC 12-5[a] ($n = 12$)
SiO_2	77.83	76.74	78.10	76.42	75.85
1σ	1.11	0.72	1.08	0.70	0.70
Fe_2O_3	1.71	1.67	1.64	1.58	1.62
1σ	0.15	0.11	0.13	0.12	0.10
Al_2O_3	13.20	12.46	13.06	12.64	12.31
1σ	0.23	0.10	0.30	0.14	0.07
CaO	0.32	0.32	0.32	0.31	0.35
1σ	0.03	0.03	0.03	0.02	0.02
TiO_2	0.16	0.16	0.16	0.15	0.18
1σ	0.06	0.02	0.04	0.05	0.05
MnO	0.06	0.07	0.06	0.06	0.04
1σ	0.04	0.03	0.03	0.03	0.03
MgO	0.07	0.08	0.07	0.07	0.08
1σ	0.01	0.02	0.01	0.05	0.02
Na_2O	3.29	4.48	3.03	2.37	2.90
1σ	0.23	0.25	0.41	0.18	0.29
K_2O	3.26	3.76	3.48	5.54	6.56
1σ	0.21	0.53	0.31	0.63	0.41
F	–	0.16	–	–	–
1σ	–	0.04	–	–	–
Cl	0.10	0.10	0.09	0.10	0.09
1σ	0.01	0.02	0.01	0.02	0.01
Total	100.20	100.68	100.00	101.36	100.75
Total-O*	93.19	97.19	93.60	95.31	95.82

[a] Previously identified as Sidi Hakoma Tuff correlates in Saylor et al. (2016).

older than the LDD-VP-1 sample. The taxonomically unassigned Burtele foot and one mandible assigned to *A. deyiremeda* (WYT-VP-2/10) come from strata overlying this tuff and are roughly contemporaneous with LDD-VP-1. The Nefuraytu mandible (NFR-VP-1/29) is younger still, recovered from <3.33 Ma strata within chron C2An.2r.

With regard to the larger Ethiopian *A. afarensis* sample, LDD-VP-1 is contemporaneous with the lower portion of the Sidi Hakoma Member of the Hadar Formation (Campisano and Feibel, 2008), and thus slightly younger than fossils deriving from the Basal Member at Dikika and the Maka Sands at Middle Awash (DIK-2-1: Alemseged et al., 2005; MAK-VP-1/2, MAK-VP-1/12 and others: White et al., 1993).

3.2. Morphological descriptions

LDD-VP-1/104—tooth fragment The specimen is likely an upper incisor fragment (lingual surface). The thickness of the enamel, as well as the pronounced nature of the basal tubercle, suggests that it represents a hominin. Its preservation does not allow detailed description.

LDD-VP-1/126–Maxilla and associated teeth This specimen preserves left and right maxilla fragments with RP^3-RP^4 and RM^2. Roots of the RM^1 and RC^1–LP^4 (lingual root) are preserved in their alveoli. It was recovered in two pieces and rejoined along the midline.

The nasoalveolar clivus is smoothly convex in sagittal and transverse planes. It is only moderately prognathic. The canine root is inclined about 73° relative to the alveolar plane (measured as described in Haile-Selassie et al., 2019). The nasoalveolar clivus passes into the nasal cavity, creating an intranasal platform (Kimbel et al., 2004). A median crest is palpable on either side of the midline. The nasal spines are damaged but would have been situated slightly inside the nasal cavity. Because the clivus continues into the nasal cavity, the estimated nasospinale-prosthion distance (24 mm) is smaller than the full length of the clivus (ca. 32 mm).

The transition between the facial and intranasal portions of the clivus is marked by a subtle change in cross-sectional contour (Fig. 2G), but no spinal crest (Gower, 1923; Kimbel et al., 2004) or other ridge is present along the inferior nasal margin. Just lateral to the midline, a shallow depression is located on the intranasal platform (more clearly developed on the right side than the left). The column of bone that forms the aperture's lateral margin blends into the subnasal surface smoothly. Combined with the lack of the spinal crest, this morphology results in an aperture with a rounded inferolateral corner.

The break along the midline reveals a medial view of the sub- and intranasal structures (Fig. 2G). The transition between the nasoalveolar clivus and the nasal floor is stepped (McCollum et al., 1993; McCollum, 2000). Preservation damage to the superoposterior portion of the clivus precludes description of contact with the vomer. The hard palate is anteroinferiorly-posterosuperiorly angled. It overlaps with the clivus for a length of roughly 16 mm. Anteriorly, the hard palate is shallow (i.e., not shelved).

The central incisor juga terminate about 8 mm below the nasal margin. The lateral incisor juga are positioned just lateral to the nasal aperture's lateral margin. The canine jugum contributes to the smooth transition between anterior and lateral faces of the maxilla. The jugum ends before reaching the column of bone lateral to the aperture. A shallow linear sulcus separates the C^1 and P^3 juga. The canine fossa is a shallow depression ca. 10 mm in diameter, positioned above the premolar roots. The fossa faces primarily laterally. The root of the zygomatic process is palpable at its anterior extent, which lies at the mesial M^1 level.

In occlusal view, the canines contribute to the anterior arch, as opposed to being in-line with the cheek teeth. The central incisor roots are larger in cross-section than the lateral incisor roots. A 3-mm patch of alveolar bone between the I^2 and C^1 probably indicates the presence of a small diastema.

A large incisive foramen is visible in occlusal view, with its posterior rim located at the P^3 level. The greater palatine grooves are well marked, especially on the right side at the M^1 level where two distinct grooves are separated by a thin crest. These grooves

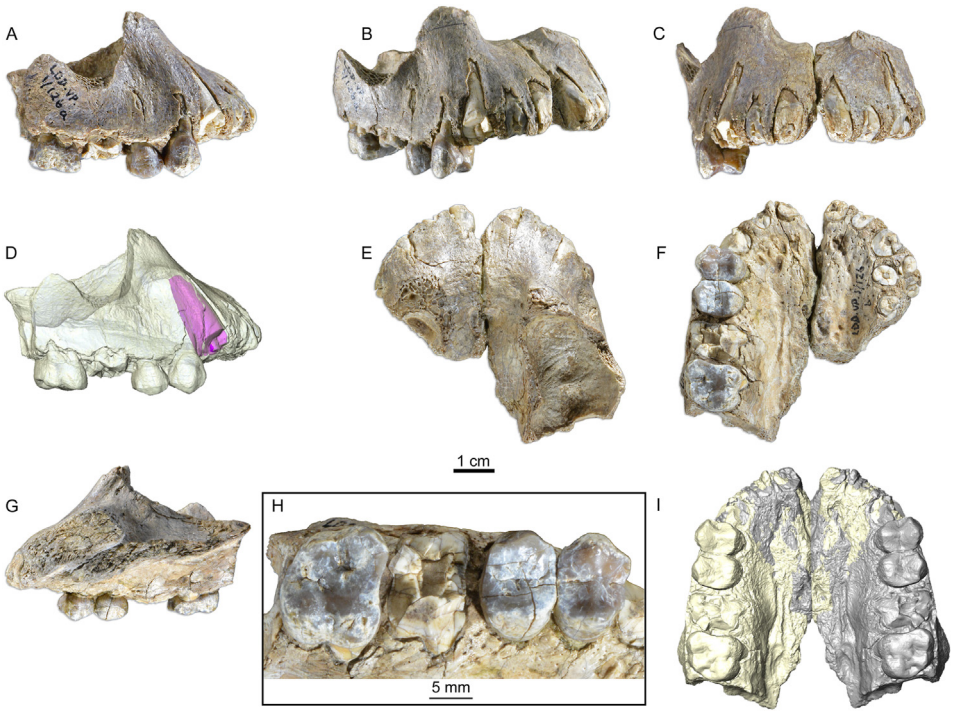

Figure 2. LDD-VP-1/126 maxilla with teeth. Shown in right lateral (A); oblique lateral (B); anterior (C); right lateral showing canine root orientation (D); superior (E); occlusal (F); and medial (G) views. In G, the right maxilla is shown unglued. Additional occlusal views show the dentition (H), and the mirror-imaged reconstruction (I). The mirror-imaged half of the reconstruction is shown in grey here and in all following figures.

converge to a depression at posterior M^2, and posterior to this depression the palatine suture is visible. The distal-most preserved portion of bone would have contributed to the greater palatine foramen.

The kidney-shaped outline of the maxillary sinus is visible on the preserved right side in superior view. Only the anterior compartment of this sinus is preserved. No pronounced subdivisions are present. The floor of the sinus is generally smooth with the exception of blunt ridges located between molar crowns.

The P^3 crown is well preserved, with the exception of slight abrasion damage to the paracone (Pa) tip. Dental dimensions are reported in Table 3. The basal outline of the crown is nearly symmetric in occlusal view (Fig. 2H). The distolingual and mesiobuccal corners are slightly rounded, but well defined. The prominence of the distolingual corner is independent of the distal IPCF, which terminates buccal to the point where the corner begins. The protocone (Pr) is positioned slightly more mesially than the Pa. The transverse crest (Tc) is prominent and interrupted by the median longitudinal groove (Lg). The median Lg is parallel to the axis of the Pa crests. An extension of the Lg indents the mesial marginal ridge (Mmr) and continues onto the mesial face, which creates a notch along the mesial contour. The posterior fovea (Fp) is larger than the anterior fovea (Fa). In lingual view, Pr wear is angular. A short mesial Pr crest forms an obtuse angle with a relatively long distal Pr crest. A series of linear irregularities are visible on the lingual surface, positioned in the center and cervical half of the crown. A mesial lingual groove begins about 1 mm above the cervix and flares out in a V-shape toward the occlusal fovea and a distal buccal groove is also present. In buccal view, the crown flares gently occlusally. The cervical enamel line is convex and centered over the mesiobuccal root. The preserved height of the Pa (measured as the maximum distance between the cervical enamel line and the cusp apex) is 10.0 mm. The mesial buccal groove is V-shaped. A weak distal buccal groove is also present and linear in form. In mesial view, the buccal wall is vertical and the lingual wall inclines slightly toward the occlusal surface. The Pa is taller than the Pr, though the discrepancy in cusp height is not large. The minimum height of the Mmr is 3 mm, as measured from the cervical enamel line to the occlusal rim. Examination of CT slices reveals that there are three fully separate roots and canals. Two roots are located buccally and have irregular ovoid shapes in cross section, and one root is lingually positioned (type 3-A-5).

The P^4 crown is fully preserved. Three fossilization cracks run buccolingually (BL) and mesiodistally (MD) across the Pr. The Pa and Pr occupy similar MD positions and both are mesially offset relative to the MD length of the crown (Fig. 2H). The basal crown outline is a MD-compressed oval in occlusal view. The MD length of the crown is larger lingually than buccally. There is no Tc and a median Lg divides the crown into buccal and lingual halves. A remnant of the Fa is present as a linear groove on the Pa. The Mmr and distal marginal ridge (Dmr) are thin. The Pa tip is polished by wear and this wear facet is tilted slightly mesially in buccal view. The distal crest of the Pa shows no wear facet. The Pr is rounded by light wear. The Pr crests are asymmetric in lingual view. Mesial and distal slopes are discernable but much less pronounced than on the P^3. A series of vertical ridges and grooves are present on the lingual face near the distolingual corner. The distal-most groove demarcates the mesial extent of a small column of enamel that approaches but does not reach the occlusal rim. In buccal view, the crown flares strongly occlusally. A mesial buccal groove is absent, but a moderately developed distal buccal groove delineates a distal flange that continues to the occlusal surface as an incipient distobuccal cuspule. The curvature of the cervical enamel line is tighter on the P^4 than on the P^3 (i.e., more V-shaped that parabolic). A weak enamel bulge is present basally. In distal view, the buccal face is upright and the lingual face is only very slightly inclined. A large rectangular IPCF is present on the distal face. Two roots are visible in the CT scan, each with one canal (type 2-A-2). The buccal

Table 3
Dental dimensions for LDD specimens. Preserved dimensions are reported first and corrections for wear and damage are given in parentheses a line below, where necessary. L, left; R, right; Avg, left and right sides averaged.

LDD-VP-	I^1		I^2		C^1		P^3		P^4		M^1		M^2	
	MD	LaL	MD	LaL	MD	LaL	MD	BL	MD	BL	MD	BL	MD	BL
1/126							8.4	12.4	8.9	12.9	–		11.6	14.3
							(8.7)		(9.3)		(11.7)[a]		(12.4)	
1/248														
L					10.7	10.1			8.9[b]	12.7				
									(9.2)					
R	9.0[c]	7.4	6.3[c]	7.5	10.4	10.8	8.2	12.8			12.5[d]			
					(10.6)		(8.8)							
Avg					10.7	10.5	8.9	12.8						
1/775[e]											12.0	14.3		
											(12.4)			

LDD-VP-	C_1		P_3		P_4		M_1		M_2		M_3	
	MD	LaL	MD	BL	MD	BL	MD	BL	MD	BL	MD	BL
1/167							12.7	11.9				
							(12.8)					
1/406											12.0	10.3
											(12.2)	
1/672	7.3	8.9	8.4	9.5	8.5	9.2	11.5	10.9	13.3	11.9		
	(7.8)	(9.2)			(9.5)		(11.6)					
1/732											14.8	13.0
											(15.1)	
1/764								15.0				
								(13.8)				
1/1065											12.6[c]	12.3[c]
											(13.6)[c]	

[a] MD of missing M^1 estimated from the space between P^4 and M^2 crowns.
[b] The LDD-VP-1/248 LP^4 crown is expanded due to fossilization cracks. The expansion primarily affects the MD dimension. The MD measurement was taken slightly buccal to crown center, where the expansion effect is marginal. It represents a minimum MD dimension.
[c] Preserved dimension is very damaged or worn. These values are not included in comparative analyses.
[d] MD of missing M^1 estimated from preserved roots.
[e] Specimen could be an M^1 or M^2.

root presents grooves both lingually and buccally, producing a butterfly-shaped cross-section.

The M^2 crown is well preserved with the exception of the enamel on the buccal face, which is weathered and abraded. The crown has a trapezoid occlusal outline (Fig. 2H). The mesial IPCF excavates the mesial contour, including most of the Mmr. The Pr is by far the largest cusp; Pa and hypocone (Hy) are subequal in size and metacone (Me) is the smallest cusp. The rounded ridge running between the Pr and Me is incised by a Lg that continues to the Fp. The Dmr is thick and faint grooves delimit a single distal cuspule. Vertically oriented ridges are present on the lingual aspect of the Pr, but these lack the shelf- or tubercle-like development of a traditional Carabelli feature and they are located just below the occlusal rim rather than closer to the cervix. In distal view, the lingual and buccal faces are upright and cusp tips are situated marginally. The distal IPCF is rectangular and positioned just below the occlusal rim, which indicates that the M^3 was in full occlusion. A faint obliquely oriented ridge is present on the buccal face of the Pa. The buccal groove is deep near the occlusal rim and continues to the cervix as a subtle linear indentation.

LDD-VP-1/131—Partial mandible and LM_3 fragment The specimen is an edentulous partial mandible assembled from numerous fragments. Joining surfaces are weathered, which creates minor offsets between fragments but there is no obvious plastic distortion within fragments. None of the base is preserved. A left M_3 fragment was recovered in the same immediate area. The tooth preserves the lingual portion of the crown and root, with a small piece of alveolar bone attached. It does not join to the partial mandible. A few cranial fragments were also recovered in close proximity to the mandibular fragments. However, they are too fragmentary for meaningful description and are not included in this study.

The dental arcade is somewhat V-shaped, owing to a medially positioned canine and post-canine divergence that begins as far anteriorly as the P_3 and continues to the M_3. The C_1 is positioned medial to the P_3 and the canine jugum faces anterolaterally. The incisor row is only slightly arched. The external surface of the symphysis has a fairly upright orientation and its contour is flat both transversely (Fig. 3F) and sagittally. The postincisive plane is long (21 mm, extending to the P_4 level) and inclined about 36° from the alveolar plane.

A foramen is present at the mesial P_4 level. It was likely positioned slightly above mid-corpus level (ca. 13 mm below the alveolar margin, with total depth at foramen >28 mm). Given the state of preservation, it cannot be determined whether this was a primary or accessory foramen. The ramus root is located posterior to M_1.

The LM_3 crown is broken buccal to the Lg, but the preserved portions of the buccal cusps preserve no morphology of note. The crown is lightly worn and weathered. There are hairline fossilization cracks running transversely across the protoconid (Prd) and metaconid (Med) and up the lingual surface of the Med. A larger crack runs obliquely across the crown's distal face. The enamel is chipped away along most of the cervix. The mesial fovea is linear and oriented perpendicular to the mesial Lg. The mesiobuccal groove is positioned slightly mesial to the lingual groove and the Med contacts the hypoconid (Hyd) via a ridge of enamel. Just distal to this ridge, two grooves delineate a large C6. No C7 is present.

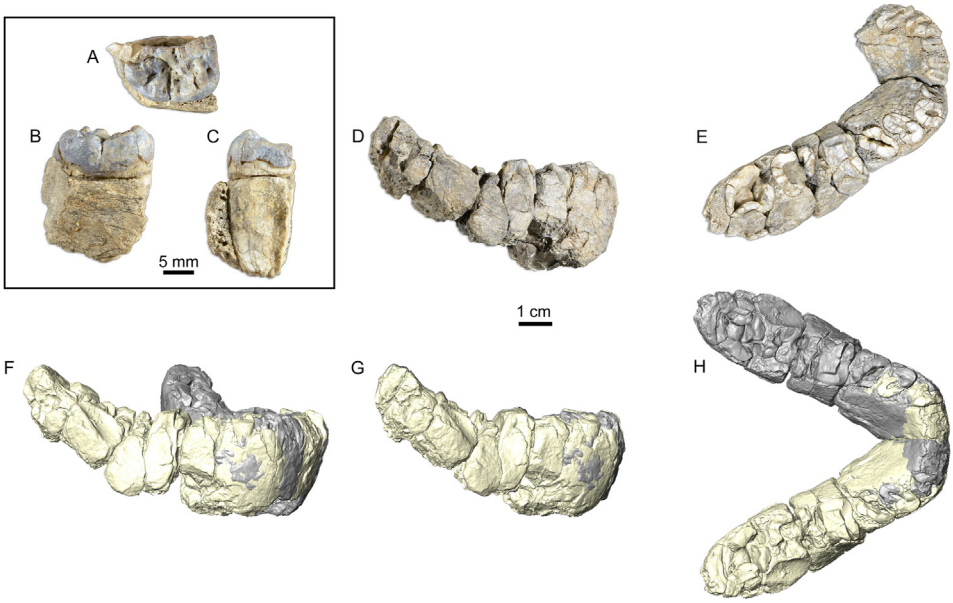

Figure 3. LDD-VP-1/131 edentulous mandible and associated LM_3. (A) Occlusal view of M_3, where mesial is to the right; (B) lingual view; (C) mesial view. (D) Right lateral view of edentulous mandible; (E) occlusal view; (F) oblique lateral view of mirror-imaged reconstruction showing transversely flattened symphysis; (G) reconstruction in right lateral view; and (H) reconstruction in occlusal view.

LDD-VP-1/167—Right mandible fragment and M_1 The specimen is a fragment of a right mandible preserving the corpus, I_1 through mesial M_2 roots and an M_1 crown. The symphyseal midline is not preserved. The plane of breakage is oriented obliquely, such that the preserved portion of the base is further removed from the midline than at the alveolar margin (Fig. 4F).

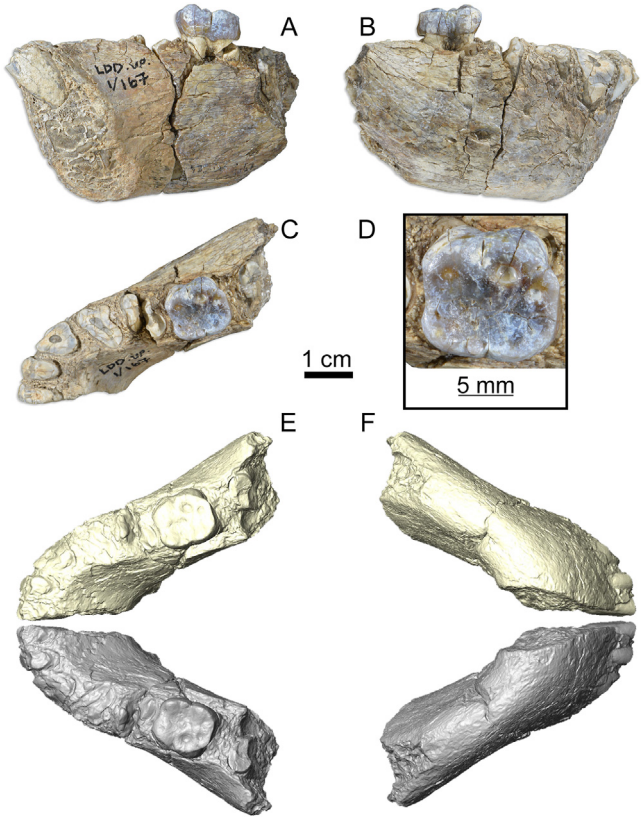

Figure 4. LDD-VP-1/167 right mandible and M_1. Shown in medial (A); right lateral (B) and occlusal (C) views. Additional occlusal views show the M_1 (D) and the mirror-imaged reconstruction (E). A basal view of the mirror-imaged reconstruction is shown in (F).

The naturally broken surface reveals a moderately sloping symphyseal cross-section near the midline (Fig. 4A). The internal surface of the symphysis presents superior and inferior transverse tori, which extend to the mesial P_4 and the P_4/M_1 levels (respectively). The tori are separated by a genioglossal fossa. The postincisive plane is 15 mm long.

The lateral surface of the corpus presents two foramina. The mental foramen is positioned between the P_4 and M_1, is set very low (17.8 mm below the alveolar margin, total depth at foramen 30.5 mm) and opens anteriorly. An accessory foramen is present 15 mm below the alveolar margin, between the premolars, and opens superiorly.

In lateral view, the basal margin is roughly parallel with the alveolar margin between the canine and M_1. The anterior root of the ramus is indicated by a slight swelling at the M_2 level and the oblique line is present distal to the M_1 crown. The location of these structures indicates a high position of the ascending ramus root.

An alveolar prominence is present on the lingual surface of the corpus, although it is weakly expressed. The subalveolar sulcus undercuts the prominence. Within this sulcus, the anterior subalveolar fossa is present as a circular depression below mesial M_1. The base is clearly everted, beginning at the M_1 level (Fig. 4F).

The RM_1 crown has a number of hairline fossilization cracks, but these do not substantially alter crown dimensions. The enamel is acid-etched. The crown has seven cusps: the standard five, a C6 and a C7. A moderate degree of wear renders occlusal basin features indistinct. The Prd contacts the entoconid (End). The deepest point in the occlusal basin is located at the junction of the longitudinal, lingual and mesiobuccal grooves. Circular dentine exposures are present on the buccal cusps. The lingual groove incises the lingual occlusal rim and lingual surface, creating a bilobate lingual contour. In lingual view, the C7 apex is well distinguished. The Med maintains pronounced relief at this wear stage. In mesial view, the buccal face is only slightly sloping and the lingual face is upright. Large IPCFs are present mesially and distally. A protostylid is

present on the buccal face of the Prd. It is obliquely oriented (1–2 mm below the occlusal rim) and extends from the mesiobuccal corner to the mesiobuccal groove. The buccal face of the Hyd and associated root curve around the distobuccal corner to the distal face, where a vertically oriented groove separates these structures from a distally projecting Dmr.

The P_3 mesiobuccal root has a single canal and the distal root is plate-like with two canals at mid-root, but bifurcates at the root tip (type 3-A). The P_4 root has two canals in the both plate-like mesial and distal roots (type 4-A).

LDD-VP-1/248—Maxilla and associated teeth This specimen comprises left and right maxilla fragments and associated teeth. The advanced degree of wear on the canines, incisors and premolars suggests that this specimen represents an old individual. The deep canine fossa may also be related to the advanced developmental age. The more complete right maxilla preserves parts of the sinus, sub- and intranasal regions, palatine and alveolar processes and matrix-filled alveoli of I^1–P^3, roots of P^4–M^2, and the mesial wall of the M^3 alveolus. The left maxilla preserves portions of the sub- and intranasal regions and I^1-I^2 alveoli.

Both halves are weathered along the midline break. The closest join occurs in the region of the intranasal and facial portions of the clivus, but the join here is imperfect. Only a small portion of the right maxilla's hard palate actually preserves the midline suture. The portion of the palatine process that would have covered the incisive canal is missing. The associated teeth include an I^1, RI^2, R and L C^1s, RP^3 and LP^4, and additional root and crown fragments. An additional upper premolar crown fragment was also recovered, but its serial allocation cannot be determined with confidence.

The inferior nasal margin is not strongly marked, but a slight crest is palpable toward the rounded inferolateral corner. This crest is continuous with the lateral edge of the nasal aperture. The bony column lateral to the nasal aperture faces more laterally than anteriorly. The strong canine jugum does not contribute to the column but instead terminates immediately below it.

A deep canine fossa is present in lateral view. The fossa occupies some of the lateral surface of the maxilla above the premolars, but also excavates the anterior face of the zygomatic root. The zygomatic root is positioned at mesial M^1. The external alveolar margin is heavily damaged, but is preserved in its original state at P^4/M^1 and at M^1/M^2. Judging from these two preserved points, the margin would have curved strongly upward moving distally along the tooth row.

A medial view (Fig. 5D) reveals a stepped transition between clivus and hard palate. The clivus continues into the aperture for a distance of about 7 mm. The hard palate has a pronounced anteroinferior–posterosuperior orientation, which creates a palate that is shallow anteriorly, but deepens posteriorly.

The I^2 alveolus is smaller and more MD compressed than that of the I^1. The canine alveolus is medially offset relative to the P^4–M^2 roots. The maxillary sinus is kidney-shaped in superior view, but detailed description of its divisions is precluded by an adhering calcareous matrix.

The I^1 crown is heavily worn and damaged. Siding cannot be determined with certainty, but preserved morphology suggests that it is a right. Anatomical directions follow this tentative siding. Enamel has flaked off the crown's distal face and a chip of enamel and dentin has been sheared off the mesial face. The root is preserved for a few millimeters below the enamel line. Fossilization cracks run along the tooth's long axis. The crown's basal outline is a labiolingually (LaL) compressed oval. A distal groove is present on the lingual face, but no median lingual ridge is preserved and a basal tubercle is absent (though this may be due to the advanced wear state). The distal marginal ridge flares slightly distally toward the occlusal surface. A shallow indentation runs vertically down the center of the labial surface (crossing root and crown), similar to the indentations that occur on some *Gorilla* central incisors. The root is roughly circular in cross-section and measures 9.2 MD by 7.5 LaL. The preserved portion of the occlusal wear surface is horizontal both LaL and MD. Dentin exposure measures 7.2 mm MD and a maximum of 3.3 mm LaL. The dentin surface is LaL wider at its mesial extent and becomes LL narrower moving distally.

The I^2 crown is heavily damaged. The mesial half of the labial face is missing as well as the mesiolingual and distolabial corners. Two major fossilization cracks run vertically through the crown, splitting it into three parts (labial, mesiolingual, and distolingual) in occlusal view. Very little of the occlusal surface is preserved, but the root is complete. A circular depression is present on the distal surface of the root, and small flakes of bone around its rim suggests the damage was associated with inward crushing. The lingual face is slightly concave, with a weakly developed gingival eminence. Most of the Dmr is preserved and it angles strongly distally. Just mesial to the ridge is a distal lingual groove. The enamel line is

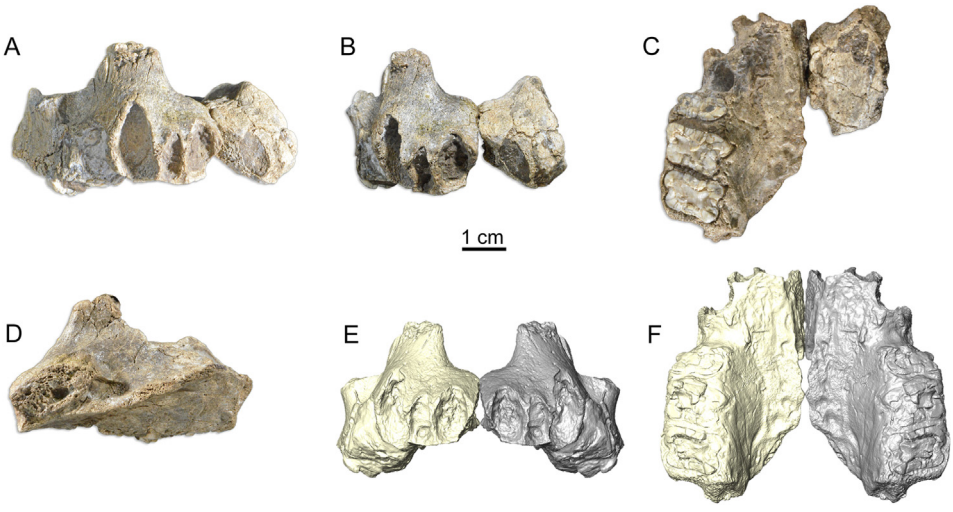

Figure 5. LDD-VP-1/248 maxilla. Shown in oblique lateral (A); anterior (B); occlusal (C); and medial (D) views. In D, the right maxilla is shown unglued. The mirror-imaged reconstruction is shown in anterior (E) and occlusal (F) views.

convex rootward and has a pinched apex that is offset distally. No IPCFs are present on the preserved on the distal surface, but presence/absence cannot be determined with certainty due to preservation damage. The root is strongly MD compressed. In distal view, the labial surface of the root is strongly convex and the lingual surface less so. The root is bluntly rounded at its apex. Root length is 17.2 mm, as measured labially from root apex to enamel cervix.

Both canines are preserved. The crowns are intact but heavily worn. The lingual face presents a vertically oriented Mmr, whereas the Dmr projects distally. The mesial shoulder extends further apically than the distal shoulder. The median lingual ridge is blunt and slightly mesially offset. The distal half of the lingual face is occupied by a slightly concave V-shaped surface. The gingival eminence is only moderately developed and has a cingulum-like form (as opposed to a more pronounced basal tubercle). A distal IPCF is present as an elongated surface on both canines. It is located on the distal face of the distal shoulder on the right canine but is more lingually positioned on the left side, where it occupies much of the Dmr. This suggests that the left and right canines had slightly different positions in the tooth row, which may relate to their different states of wear. The root is thick, squat, and ends in a blunted point. A longitudinal groove is present on the mesial surface and more pronounced on the left canine than on the right. Root lengths measure 24.0 mm (right) and 24.5 mm (left). Wear is considerably less advanced on the right side. Exposed dentin has an irregular diamond shape, with distal apex longer than mesial apex (maximum dimension 5.5 mm). The right canine exhibits three occlusal wear facets that are continuous, but distinct in orientation. The apical wear facet is occlusally concave and oriented horizontally (Fig. 6, Labial). It extends as a mesially facing facet that runs down the mesial crest to contact the mesial shoulder (Fig. 6, Labial and Mesial). The third facet runs along the lingual surface of the distal crest (Fig. 6, Lingual). The left canine represents wear at a more advanced stage. Here, one wear facet occupies most of the crown. This facet is occlusally concave in labial view. Wear facets along the mesial and distal crests are affected by the advanced state of occlusal wear. The mesial crest is no longer present and the facet along the distal crest is very small (ca. 1.5 mm long) polished surface on the lingual face of the distal crown shoulder.

The RP^3 is complete, but traversed by a few fossilization cracks. The most prominent of these runs MD along the median Lg and another bisects the Pr. The roots are nearly complete, except the tip of the lingual root. The P^3 crown is BL elongate. In occlusal view, the buccal and lingual faces are convex and symmetric. The mesial contour is slightly concave and the distal contour is flattened due to strong IPCFs. A lunate-shaped groove is present just distal to the Mmr, representing the remnant of the Fa. Other aspects of the fissure pattern have been erased by wear. Wear is most pronounced on the distal aspect of the Pr, exposing a comma-shaped patch of dentin that measures 4.3 mm MD. The Pa is blunt and flattened but shows no clear wear facets. In lingual view, wear on the Pr can be separated into mesial and distal crests. The distal crest is very steep and occupies most of the cusp's length (Fig. 6, Lingual). The mesial crest is comparatively short and more horizontal. In mesial view, the lingual wall slopes gently inward moving occlusally and the buccal wall is comparatively upright. The mesial IPCF is lunate in shape and is positioned buccal to the midline. It measures 4.9 mm BL. The distal IPCF occupies the entire distal face of the crown. It has a long rectangular shape and measures 6.8 mm BL. The Pa tip is rounded but mesial and distal crests can be distinguished in buccal view. The mesial crest is shorter. Mesial and distal buccal grooves are present. Both are linear in form and only moderately developed. The tooth is two-rooted and both roots are stout. The buccal root is fused from two elements separated by a strong groove. A CT scan shows that the buccal root contains two separate pulp cavities

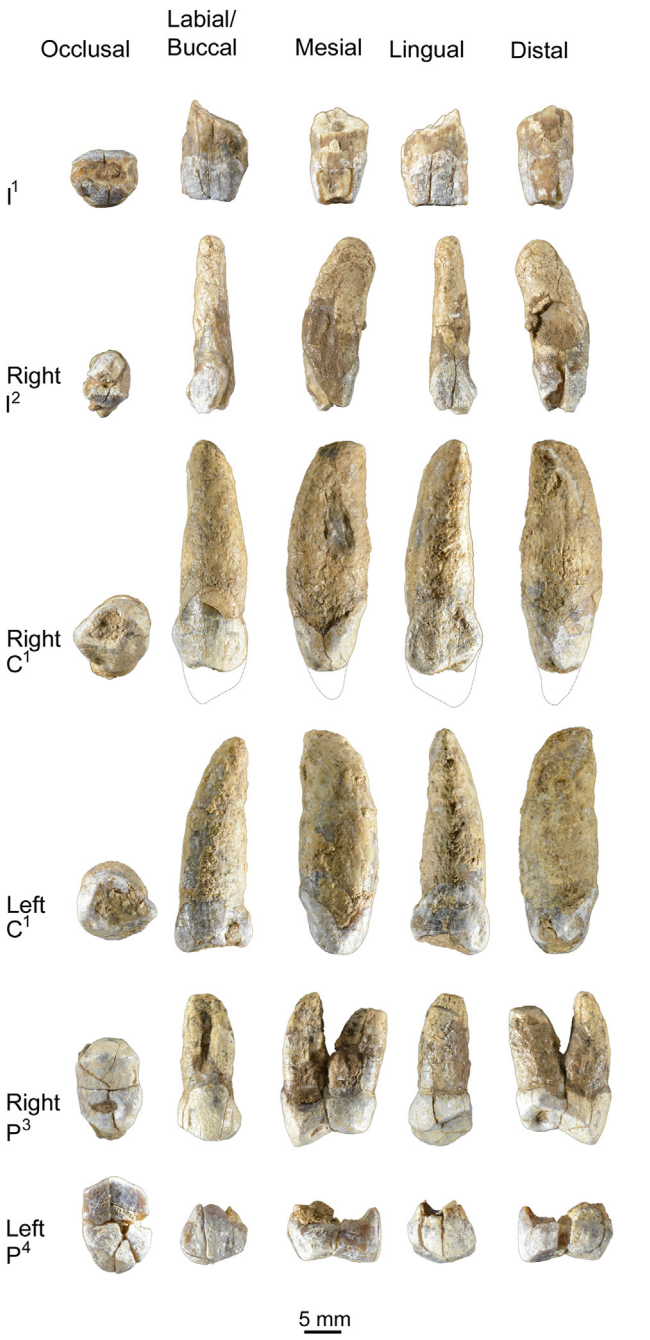

Figure 6. LDD-VP-1/248 tooth crowns. In occlusal views, labial or buccal is toward the top of the image.

apically. At mid-root, the buccal root is teardrop-shaped in cross-section and the lingual root is a MD compressed oval.

The P^4 crown was reconstructed from six fragments and is nearly complete. The root is not preserved. The basal outline of the crown constitutes a BL elongated oval. The occlusal rim departs from the basal contour mesiolingually, giving the occlusal fovea a more square-like shape. The mesial and distal crown contours are perpendicular to the Pa crests in occlusal view. Two linear grooves are present on the occlusal surface, paralleling the buccal half of the Mmr. Additional features on the occlusal surface are obscured by wear. Flat, polished wear facets are present on the mesial Pa crest and at the distobuccal corner, but no enamel is exposed. In buccal view, the crown tapers strongly toward the cervix and the cervical

enamel line is V-shaped. A mesial buccal groove is present but a distal buccal groove is not. In mesial or distal views, the buccal wall is upright, whereas the lingual wall slopes toward the crown center. The mesial IPCF is lunate in shape and restricted to the buccal half of the crown, whereas the distal IPCF occupies the BL extent of the distal face. In lingual view, an angular wear pattern is present on the Pr. The distal wear slope is longer and steeper than the mesial. A similar pattern is present on the P^3, but the P^4 wear pattern is not as strongly asymmetric (Fig. 6, Lingual). The right P^4 root is present in the maxilla. Two separated roots and pulp canals are present at mid-root level (type 2-A-2). The buccal root presents grooves both lingually and buccally, producing a butterfly-shaped cross-section.

LDD-VP-1/406—RM_3 This is a very small, complete M_3 crown lacking its roots. One hairline crack runs BL across the Prd and a second crack runs down the MD axis, buccal to the Lg. The occlusal outline is an elongated oval that narrows distally. Six cusps are present: the standard five and a well-defined C7. The mesial and distal portions of the Lg are very lingually offset, so that the buccal cusps occupy much more than half of the total crown area. The mesial Lg is lingually concave, which creates a narrow V-shaped lingual extension to the Prd that contacts the C7. This contact point marks the deepest point in the occlusal basin. The hypoconulid (Hld) is very large, second only to the Prd in area. Examination of a CT scan allowed us to confirm that no C6 is present on this worn crown, because there is no dentin horn present between the End and Hld (Skinner et al., 2008). No Fp is discernable. Instead, the distal Lg extends to meet the distal crown margin.

Three distinct cusps are visible in lingual view. The Med is the tallest cusp at the current wear stage. Its distal crest is long and strongly slanting, whereas the C7 and End tips are rounded.

The mesial buccal groove incises the buccal face deeply near the occlusal rim and continues as a more subtle linear indentation that fades out before reaching the cervix. The distal buccal groove is a subtle linear indentation.

An IPCF is present mesially but not distally. The buccal cusps are flattened while the lingual cusps maintain relief (Fig. 7, top). Although the buccal cusps are nearly flattened by wear, no dentin is exposed.

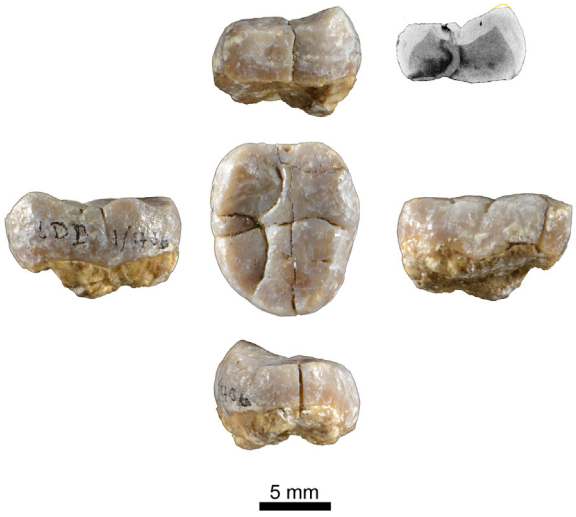

Figure 7. LDD-VP-1/406 RM_3. Occlusal view is shown in the middle. Clockwise from top: mesial view, cross-sectional CT slice through protoconid and metaconid dentin horns, buccal view, distal view, and lateral view.

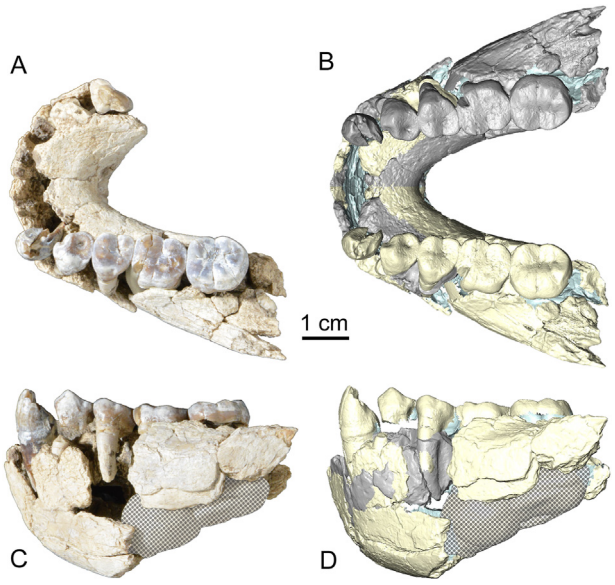

Figure 8. LDD-VP-1/672 mandible. (A) Occlusal view; (B) occlusal view of mirror-imaged reconstruction; (C) left lateral view; (D) left lateral view of mirror-imaged reconstruction. In C and D, grey hatching overlies molding material temporarily supporting joins among the different pieces of the specimen.

LDD-VP-1/672–mandible and teeth The specimen consists of a mandibular corpus that has been reassembled from numerous fragments, complete crowns of LC_1–LM_2, fragments of the right premolars, and additional incisor and molar fragments of indeterminate position (Figs. 8 and 9). The original bone surface has flaked away to variable degrees across the corpus. Chemical weathering and acid etching occur on all tooth crowns (the C_1 and LP_3 are particularly affected).

The mandibular corpus consists of two non-adjoining pieces. The larger of these preserves the dental arch from the RP_4–LP_4 and the internal alveolar margin from LM_1–LM_2. The smaller piece of the corpus consists of the external alveolar margin along LM_1–LM_2 and part of the ramus root. Although the two corpus pieces do not join to each other, the specimen can be reassembled by joining the post-canine dental row across the well-developed IPCFs and aligning the crowns with tooth roots and the alveolar margin at their appropriate positions. The alveolar margin is heavily damaged. Most of the symphysis is preserved, but a fragment is missing from the genioglossal fossa and surrounding region. The basal contour is preserved without distortion between right and left P_3s.

The canines and incisors are arranged in a tight, anteriorly convex arc. The mesial root of the P_3 marks the transition between the lateral and anterior corpus and the canine is set medial to the P_3. The internal surface of the symphysis presents a short post-incisive plane (ca. 8 mm) oriented ca. 30° relative to the alveolar plane. The superior transverse torus is weakly expressed. The presence of a genioglossal fossa can be inferred from preserved regions. The inferior transverse torus is elevated ca. 6 mm from the base. The transverse tori continue onto the medial surface of the corpus. The superior torus loses its definition at the distal P_3 level, whereas the inferior torus extends further posteriorly, to the mesial P_4 level. Although the base is not preserved along the molar row, it is clear from the slope of the medial wall of the corpus that the base would have been considerably everted.

Morphology of the lateral aspect is partially preserved only on the left side in the premolar region. A foramen is preserved at the P_3 distal root, positioned roughly at mid-corpus. It is likely the primary

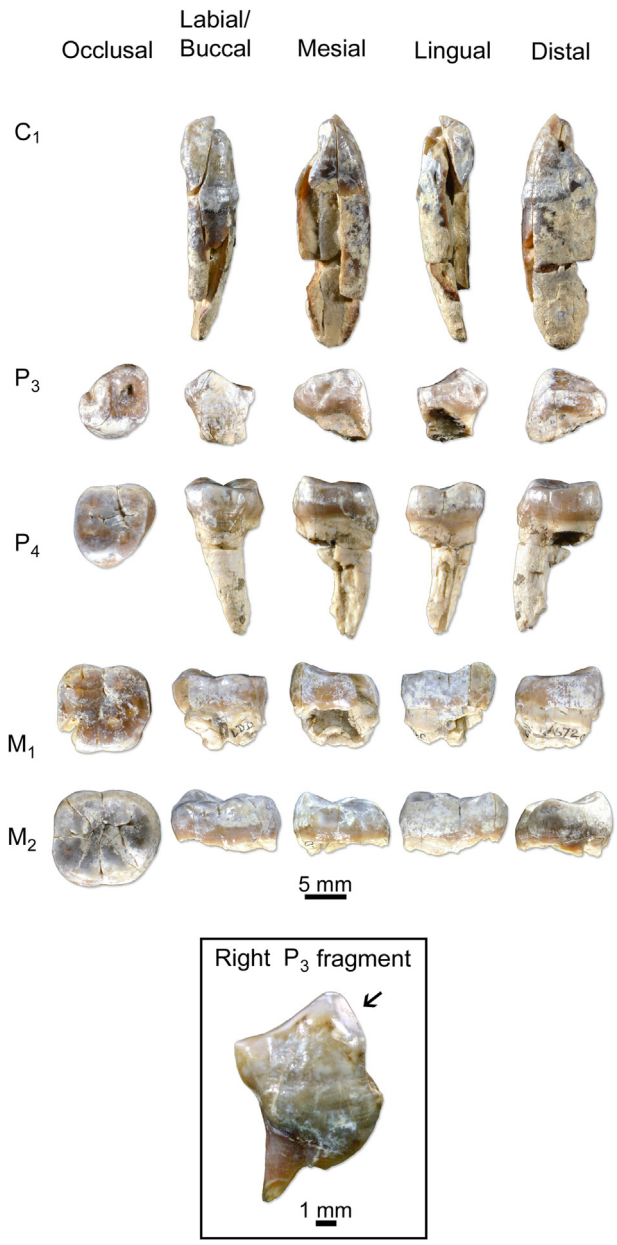

Figure 9. LDD-VP-1/672 teeth. Crowns are from the left side, except where otherwise indicated. In occlusal view, lingual is toward the top of the image. The arrow in the inset indicates the location of a contact facet on the RP_3.

mental foramen, but it could also be an accessory foramen. This identification cannot be determined with certainty due to the missing portions of the corpus. The bone surface is too heavily flaked to judge the direction in which the foramen opens. The presence or absence of a lateral corpus hollow cannot be assessed due to insufficient preservation.

The ramus root extends to the mesial M_1 level. The oblique line begins to curve superiorly near the middle of the M_2 crown, indicating an anterior position to an ascending ramus that would have covered the M_3 in lateral view. The ramus root is set quite high on the corpus, about 4.5 mm below the alveolar margin.

The C_1 has been pieced together from three fragments. The crack that bisects the crown into mesial and distal halves joins tightly at the dentine interface, with a small gap (0.15 mm) at the enamel surface labially and a larger gap lingually (0.5 mm). Pieces of enamel and dentine are missing from the center of the lingual face and from the crown tip (the distal half in particular). The enamel cap is also missing from the distal tubercle. The occlusal outline of the crown is a MD-LaL elongate oval with a flattened mesial face. The lingual surface is damaged, so the presence of a vertical median ridge cannot be assessed. However, the mesial half of the lingual face is flat, which suggests that if the lingual ridge were present, it would have been distally placed. A small portion of the distal vertical groove is preserved as a sharply incised linear feature, just mesial to the distal tubercle. The mesial crown shoulder is upright and ends just below the mesial occlusal crest. The distal tubercle is set low—it would have extended only about 3 mm above the cervix. A weak mesiolabial groove is present on the apical half of the crown. Two linear hypoplastic defects are present within 3.5 mm of the cervix. The complete length of the root is preserved and measures 17.5 mm from the lowest-most extension of the cervix to the root apex. The crown possesses distinctly angled wear facets. The mesial crest is slightly inclined and short compared to the distal crest. Only a small part of the distal crest is preserved (best seen in distolingual view). Here, a narrow strip of dentin is exposed from wear with the upper canine. Where the enamel cap is broken away from the distal tubercle, the relationship between worn enamel and dentine can be seen in cross-section.

The LP_3 crown is intact. It has a roughly triangular occlusal outline, with a lingually projecting distolingual corner. The Prd is worn and rounded but no dentin is exposed. Wear has also flattened the distal segment of the Dmr. The internal structures of the crown (Prd crests, Tc, etc.) are set orthogonal to the postcanine tooth row. In occlusal view, the convexity of the buccal surface arches evenly across the length of the Prd crests. The Prd lies near the buccal margin of the crown. A Med is present, although considerably smaller and shorter than the Prd. A well-defined Tc connects the two cusps, and divides the Fa from a comparatively large and rectangular Fp. No Lg is present. The Fa is somewhat open, due to a groove that divides the mesial segment of the Mmr from the poorly developed lingual segment. The Dmr is thick and no accessory cuspules are discernable. The Fa appears somewhat diamond-shaped in lingual view (*sensu* Delezene and Kimbel, 2011), with the mesial protoconid crest and Tc forming the top portion of the diamond and the bottom portion formed by the non-continuous mesial and lingual segments of the Mmr. The groove interrupting the Mmr does not continue all the way down to the enamel line. A short distal metaconid crest gives rise to the lingual segment of the Dmr, which is elevated ca. 4 mm above the enamel line. A facet indicating contact with the C^1 is present on the buccal face, just below the mesial protoconid crest. The facet is difficult to see on the LP_3, because the enamel surface is especially damaged here. However, a fragment of the RP_3 is also preserved with less damaged enamel and this tooth presents the same morphology (Fig. 9, inset). The enamel line traces a rounded 'V' shape along the buccal surface, with the apex only slightly mesially offset. The enamel line extends much further rootward on the buccal surface, compared with the other crown surfaces. A distal buccal groove is present. In distal view, the buccal face of the crown is fairly upright. An elongated oval IPCF occupies most of the distal face.

The P_4 was first described by Haile-Selassie and Melillo (2015). The occlusal contour is rhomboid in shape, with a distally projecting distolingual corner and abbreviated distobuccal corner. The occlusal surface presents three well-defined cusps. The Prd is the largest and Med and End are roughly equal in size. The Prd and End are separated by the transverse lingual groove, which continues down the lingual crown face. The buccal transverse groove and an accessory fissure delineate an incipient Hyd. The Prd and Med are aligned and positioned mesially. This cusp position, in combination with a thick Mmr, limits the Fa to a tiny pit at the mesial extent of

the median Lg. Transverse crest morphology cannot be assessed in detail due to wear, but even in its worn state, the transverse crest sits slightly above the level of the Mmr. The crest is incised by the median Lg. The Fp occupies much of the occlusal basin. It is formed via contributions from all of the cusps and is slightly lingually offset. One minor fissure arising from the Fp courses directly distally and another distobuccally. These fissures do not incise the thick Dmr. In lingual view, the mesial metaconid crest is shorter and more horizontal than the distal metaconid crest. A long mesial crest is present on the End. The lingual groove extends from the occlusal rim to the cervix. A well-defined distal buccal groove is present on the buccal face, but the mesial buccal groove is absent. Hypoplastic defects cross the bottom half of the crown. In mesial view, the crown presents an upright lingual face. The buccal face is upright near the cervix, but exhibits a slight inward sloping toward the occlusal margin. IPCFs are present mesially and distally. Prd is worn flat and a tiny point of dentin is exposed. Wear on the Med is most pronounced on the mesial metaconid crest. The entire distal margin of the crown is worn flat without dentin exposure. There is light wear along the End mesial crest. The Med has maintained a well-defined apex despite flat wear and dentin exposure on the Prd.

Three cracks run across the mesial portion of the LM_1, but do not notably alter crown dimensions. The mesiobuccal corner is missing. The rest of the crown is well preserved and moderately worn, with circular dentine exposures on the Hyd and Hld. The Hld is worn flat. Lingual to this wear facet, a distinct facet is present on the distal crest of the End. The crown has a square outline with a rounded distobuccal corner and a subtle distal projection of the Dmr. The lingual groove incises the occlusal rim and lingual face, producing a bilobate contour. The same is true of the buccal face, to a lesser degree. Five cusps are present. The mesial Lg curves mesiolingually, separating the Mmr from the Med. The Prd has a distolingual extension that contacts the End. The mesiobuccal and lingual grooves are almost transversely aligned. The distal Lg extends only about 1.5 mm distally before bifurcating into the distobuccal and distal grooves. No distal fovea is apparent. In mesial view, the lingual face is upright and the buccal face slopes only slightly near the occlusal rim. The buccal cusps are worn flat, whereas the Med retains topographic relief. Large, rectangular IPCFs are present mesially and distally, both contacting the occlusal rim.

The LM_2 is complete, with hairline fossilization cracks running obliquely across the crown. This crown is similar to the M_1 in having a curved mesial Lg, contact between the Prd and End and nearly aligned mesiobuccal and lingual grooves. However, the M_2 possesses a distal fovea and a C6. The crown outline is more MD elongated than the M_1, and the M_2 lacks the distally projecting Dmr. The mesial IPCF is a rounded rectangle occupying much of the mesial face, whereas the distal IPCF is more subtle. The latter is small facet, which is buccally offset and located at near the center of the crown's height (i.e., it does not contact the occlusal rim), indicating that the M_3 of this individual was erupted but likely not fully in occlusion.

LDD-VP-1/732–LM_3 The specimen is a nearly complete LM_3 crown, with enamel missing along portions of the cervix (Fig. 10). Hairline fossilization cracks are present on the crown walls and one crosses the occlusal surface, across the Med. These cracks have no quantifiable effect on crown size.

The crown is MD elongated and possesses a relatively narrow talonid. A deep mesiobuccal groove divides the Prd from the basally swollen Hyd, giving the buccal face a bilobate appearance in occlusal view. Five cusps are present. The mesial fovea is a linear feature that stretches from the lingual third of the Prd to the buccal third of the Med. It is positioned below the rest of the occlusal surface. The mesial Lg is perpendicular the mesial fovea. The mesiobuccal groove is set slightly more mesial than the lingual groove. The distal longitudinal fissure bifurcates into accessory lingual and buccal branches as it approaches the distal margin of the crown. These accessory fissures delineate a distal fovea that is enclosed by a Dmr. Although the distal ridge lies between the accessory fissures, we do not classify it as a C6 because it lacks an apex. A polished facet on the Prd and presence of a mesial IPCF demonstrates that the tooth was in occlusion.

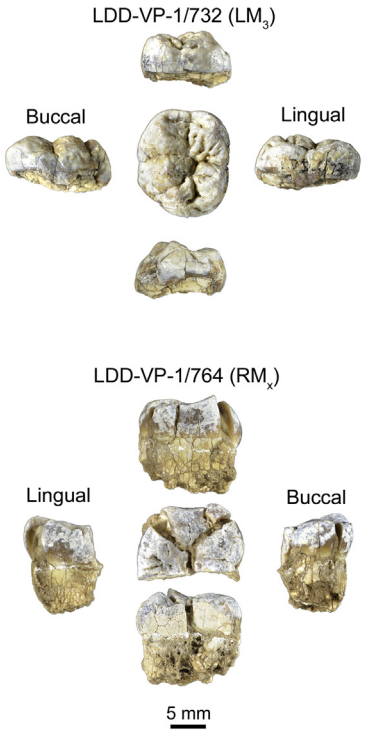

Figure 10. Isolated teeth from LDD-VP-1. Occlusal view is shown in the middle, mesial view above and distal view below. Lingual and buccal views are labeled.

A number of features are present on the buccal face. A strongly expressed protostylid occupies much of the Prd and ends at the mesiobuccal groove (Type 5 of Hlusko, 2004). The buccal face of the Hyd presents a number of vertical enamel wrinkles that are most pronounced cervically.

LDD-VP-1/764–RM_x fragment The specimen is the mesial half of a right lower molar. The large size of the tooth suggests it is either an M_2 or M_3. It is fragmented into four pieces, and these pieces are cemented together in an expanded state (Fig. 10). Crack thickness varies between 1.3 and 1.8 mm. A portion of the mesiolingual crown corner is missing. Naturally fractured surfaces reveal qualitatively thick enamel.

The occlusal surface exhibits a transversely oriented, linear mesial fovea. The mesial Lg is positioned at the crown's BL center and oriented perpendicular to the mesial fovea. The tooth is broken just distal to the mesiobuccal line, it is clear that the buccal contour is strongly bilobate. The apex of the C7 is pronounced in lingual view and positioned mesial to the lingual groove.

Protostylid development is ambiguous. An enamel groove is present mesiobuccally, near the occlusal rim. The groove runs along the distal half of the Prd and terminates at the mesial buccal groove. Because occlusal wear renders the boundary between the occlusal and buccal surfaces indistinct, it is unclear if this feature is an

accessory groove on the occlusal surface or a protostylid positioned unusually high on the buccal crown face.

Wear is moderate and there are no dentine exposures. In mesial view, the Prd is flattened and the Med is elevated. A large IPCF is present on the mesial face (5.7 BL x 3.5 superoinferiorly) that contacts the occlusal rim.

LDD-VP-1/775–LM$^{1/2}$ The specimen is a LM^1 or LM^2 in an advanced stage of wear. The buccal cusps are flattened and a large, continuous region of dentin occupies the lingual half of the crown. The tooth is broken and enamel surrounding the dentin exposure is missing from the mesiolingual corner and from the lingual half of the distal face (Fig. 11).

Wear and damage prevent assessment of most occlusal basin features. The Pa and Me are similar in size. There is a strong lingual orientation to the wear facets on the Pa and Me. The buccal wall is vertically oriented. Where enamel is preserved on the distal crown face, part of a distal IPCF is present.

A V-shaped cleft is present on the buccal face. The mesial arm of this cleft is the longer of the two. The arms of the V stretch from just below the occlusal rim to the point where they meet, at the base of the buccal groove.

LDD-VP-1/876–RM$_x$ fragment The specimen is the distal half of a right lower molar fragment (Fig. 11). The mesial break runs obliquely across the Med tip. The preserved portion of the Med and Hyd contact each other and prevent contact between the Prd and End. The mesiobuccal and lingual grooves are nearly aligned transversely. The distal Lg is roughly parallel with the crown's MD axis. The distobuccal groove deeply incises the occlusal rim and runs down the buccolingual crown wall, before fading away about half way to the cervix. The distal fovea is well defined by the End, Hld and Dmr. A C6 with a defined apex is present on the Dmr.

LDD-VP-1/1065–LM$_3$ The specimen is a left lower molar crown that has been severely acid etched (Fig. 11). The mesial IPCF is pronounced and strongly inclined from mesiobuccal to distolingual. The talonid is narrow relative to the mesial portion of the crown. The longitudinal groove is positioned at the approximate BL center of the crown and appears to divide the Hld from a similarly sized C6. Even given the damage to the crown, the pattern of wear is distinct—with the buccal cusps worn nearly flat while the Med maintains relief.

LDD-VP-1/1111—incisor fragment The specimen is half of the labial face of an upper incisor. The rounding of the occlusal edge suggests that it is the distal half. The thickness of the enamel suggests that it represents a hominin.

3.3. Comparative anatomy

The mandible is well represented for most early *Australopithecus* species and has been central to differential diagnoses. Comparative descriptions of *A. anamensis*, *A. afarensis*, and *Australopithecus africanus* mandibles focused on features that demonstrated more primitive morphology in geologically older samples (Johanson et al., 1978; Johanson and White, 1979; White and Johanson, 1982; White et al., 1983; Leakey et al., 1995; Ward et al., 2001), whereas descriptions of *A. bahrelghazali* and *A. deyiremeda* mandibles focused on features that differ from *A. afarensis* largely due to their contemporaneity (Brunet et al., 1996; Guy et al., 2008; Haile-Selassie et al., 2015). In the LDD sample, it is possible to assess features of the symphysis, lateral corpus and overall arcade shape that are discussed in the diagnoses of all early *Australopithecus* species mentioned above.

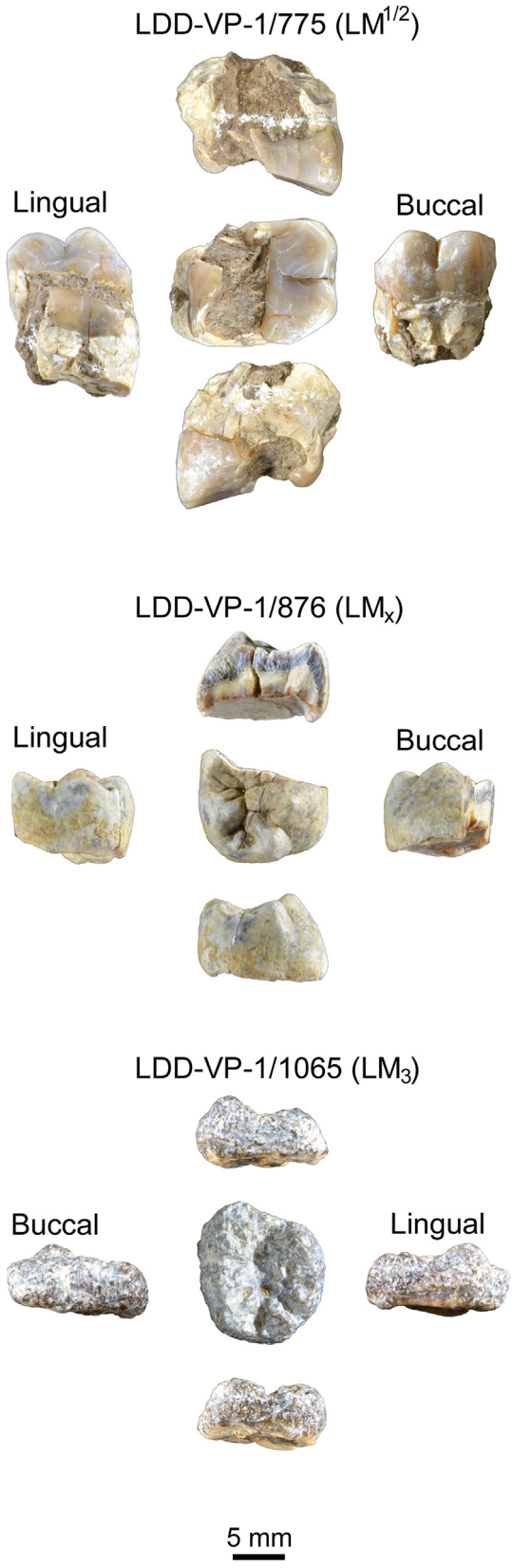

Figure 11. Additional isolated teeth from LDD-VP-1. Occlusal view is shown in the middle, mesial view above and distal view below. Lingual and buccal views are labeled.

Symphysis cross-section The original diagnosis of *A. afarensis* described the mandibular symphysis as being posteriorly inclined and possessing a rounded, bulbous external contour (Johanson et al., 1978). This description emphasized differences from the straighter, upright contour seen in *A. africanus*. The *A. anamensis* symphysis exhibits an even greater degree of inclination and is convex along the full extent of its external contour (Kimbel et al., 2004; Leakey et al., 1995; Ward et al., 2001, 2020). In comparing midline cross-sections, the 'cut-away' basal contour of *A. anamensis* has been contrasted with the 'filled out' (Kimbel et al., 2004) or 'bulbous' (Johanson et al., 1978; Kimbel and Delezene, 2009) contour of *A. afarensis*. Traces of the receding symphysis also appear in corpus cross-sections at the P_3 level, where the lateral corpus contour is inclined in *A. anamensis,* showing a particularly pronounced inferomedial sweep below the mental foramen. In contrast, the corpus contour is more vertical in *A. afarensis* (Kimbel et al., 2006). A temporal trend in these features has been proposed due to the more *A. anamensis*-like morphology of mandibles attributed to *A. afarensis* that come from Laetoli and sample older (>3.5 Ma) time intervals (Kimbel et al., 2004, 2006; but see; White et al., 2000).

The LDD mandibles possess moderately inclined symphyses (SOM Fig. S3). The LDD-VP-1/167 symphysis is inclined ca. 58° relative to the alveolar plane—qualitatively similar to *A. afarensis* specimens with steeper symphyses like A.L. 198-1 and A.L. 333w-60. The LDD-VP-1/672 symphysis is more upright. Its superior half is inclined about 68 degrees relative to the alveolar plane, whereas the inferior half sweeps more steeply toward the base (similar to A.L. 333w-12 and A.L. 207-13). The preserved portion of the LDD-VP-1/131 symphysis is oriented ca. 74° relative to the alveolar plane, qualitatively similar to A.L. 400-1a and MAK-VP-1/12. The basal portion of the symphysis (preserved in LDD-VP-1/167 and LDD-VP-1/672) shows a filled out external contour. Cross-sections at the distal P_3 reveal an especially upright lateral contour in LDD-VP-1/672, whereas LDD-VP-1/167 is slightly more inclined, but still lacks the pronounced degree of inferomedial sweep seen in *A. anamensis* specimens KNM-KP 29281 and KNM-KP 31713 (SOM Fig. S3).

Cross-sectional shape of the mandibular symphysis also played an important role in the diagnosis of *A. bahrelghazali* (Brunet et al., 1996; Guy et al., 2008). Features described as distinct in this species (i.e., short and vertical postincisive plane, shallow genioglossal fossa and deep, wide symphyseal base) are not present in the LDD sample, with the exception that the symphysis is transversely flat in both LDD-VP-1/131 (Fig. 3F) and in KT12/H1.

Mandibular corpus A number of features have come to characterize the mandibular corpus of *A. afarensis*, although their expression is variable. Main features include the presence of a lateral corpus hollow, an inferiorly positioned mental foramen, a ramus root positioned high on the corpus and arising around the M_1, and an everted base (Johanson et al., 1978; Kimbel and Delezene, 2009; Kimbel et al., 2004; White, 1977; White et al., 1983; 2000; SOM Fig. S4).

The sample of well-preserved *A. anamensis* mandibles is comparatively small but appears to share many of the features listed above. Like *A. afarensis*, the ramus root is high on the corpus and positioned around M_1, the mental foramen sits low on the corpus, and the lateral corpus hollow has been described as present (although its expression is less pronounced in the available *A. anamensis* fossil sample than in *A. afarensis*). Recently published observations hint at a further potential difference in basal eversion, but sample size remains limited (Ward et al., 2001, 2013, 2020).

Mandibles attributed to *A. deyiremeda* were differentiated from *A. afarensis* and more primitive hominins in lacking a lateral corpus hollow and in possessing an anteriorly positioned ramus root that results in a relatively broad corpus at the M_1 and M_2 levels. The ramus root was also described as having a low position (Haile-Selassie et al., 2015).

All three LDD mandibles possess a ramus root positioned high on the corpus and extending anteriorly to the mid- or mesial-M_1 level (SOM Fig. S4). Corpus dimensions of LDD-VP-1/167 and LDD-VP-1/672 fall within the *A. afarensis* range (Table 4) and do not possess the elevated corpus shape index that reflects the inflation of the *A. africanus* corpus at the P_4 level, nor the elevated index at the M_1 level that reflects the anteriorly positioned ramus root in *A. deyiremeda*. The LDD-VP-1/167 mandible shows a low mental foramen position (Table 4) and everted base (Fig. 4F), and the preserved portions of LDD-VP-1/672 suggest similar morphology. The presence or absence of a lateral corpus hollow can only be assessed in LDD-VP-1/167. A small, shallow depression is palpable on the corpus between P_4 and M_1, just above the mental foramen. However, the other structures defining the hollow (C_1 and P_3 juga, alveolar prominence, and lateral prominence) are weakly expressed, which results in a lateral surface that generally has minimal topographic relief. Although this morphological pattern is not common in the *A. afarensis* hypodigm, corpus hollowing is minimally developed in some specimens, notably in DIK-2-1 (see Discussion).

Nasal Aperture Kimbel et al. (2006, 2004) characterized nasal aperture morphology of Hadar *A. afarensis* as possessing a thin lateral margin, a sharp inferolateral corner, and either a spinal crest inferiorly or an abrupt change in clivus contour that delineates the sub- from intra-nasal surfaces. These structures occupy a single plane and define the limits of the aperture. The single noted exception to this morphological pattern in the *A. afarensis* hypodigm is the Garusi maxilla from Laetoli (Puech et al., 1986; Kimbel et al., 2004), and it is also absent in *A. anamensis* (Haile-Selassie et al., 2019; Ward et al., 2001, 2020). One hypothesis that follows from these observations is that the more sharply delineated aperture was absent in *A. anamensis* and evolved over time to become fixed in later *A. afarensis* populations at Hadar. In this framework, the lack of the sharply delineated aperture in the Garusi maxilla reflected its temporal proximity to *A. anamensis*.

Our observations ally the LDD maxillae more closely with the Hadar sample. Although neither of the LDD maxillae possess a spinal crest, there is a contour change of the clivus coincident with the aperture that is not present in *A. anamensis* (SOM Fig. S5). The aperture's inferolateral corners are more clearly defined in the LDD maxillae than in *A. anamensis* maxillae, but not as sharp as in some Hadar specimens.

Configuration of nasoalveolar clivus and hard palate Configuration of the nasoalveolar clivus and hard palate differs between *A. afarensis* and later species (SOM Fig. S5). *Australopithecus afarensis* is characterized by an anteroinferior to posterosuperiorly inclined clivus, an extensive intranasal platform, and a stepped entrance to the nasal cavity (McCollum et al., 1993; McCollum, 2000; Kimbel et al., 2004). The palate was initially described as shallow anteriorly and only moderately deep posteriorly (Johanson et al., 1978; White et al., 1983), but more recent work recognized greater variability in both aspects of palate depth (Lockwood and Tobias, 1999; Kimbel et al., 2004).

Australopithecus africanus, in contrast, exhibits less of an intranasal platform, a higher frequency of anterior shelving and greater average palate depth (Lockwood and Tobias, 1999; Kimbel et al., 2004). Haile-Selassie et al. (2015) noted that the *A. deyiremeda* holotype, BRT-VP-3/1, exhibits little overlap

Table 4
Corpus dimensions in LDD mandibles and comparative samples. Comparative data from Kimbel et al. (2004), Ward et al. (2001), Haile-Selassie et al. (2015, 2016a) and collected by the authors in this study. Statistical summaries include estimated measurements. A list of comparative specimens is provided in SOM Table S2.

Specimen	At P_4			At M_1			Mental foramen
	Height	Breadth	Shape index	Height	Breadth	Shape index	Height index[a]
LDD-VP-1/167	31.8	17.5	55.0	29.4	18.3	62.2	41.6
LDD-VP-1/672	33.8	19.3	57.1	–	–	–	–
A. anamensis							
N	3	3	3	5	4	3	2
Mean	36.5	20.1	55.6	34.1	19.0	55.6	49.3
SD	6.0	1.3	6.1	6.7	2.3	6.1	2.0
Range	31.5–43.1	18.5–20.9	48.5–59.5	26.0–41.0	17.0–22.0	48.5–59.5	47.9–50.8
A. afarensis							
N	21	27	21	25	29	21	23
Mean	36.6	19.3	52.9	34.2	20.0	52.9	45.0
SD	4.8	2.4	5.3	4.1	2.2	5.3	5.8
Range	28.0–44.0	15.8–25.0	44.4–67.5	27.8–41.3	15.8–24.7	44.4–67.5	36.5–60.7
A. deyiremeda							
WYT-VP-2/10	35.7	23.8	66.7	34.3	26.2	76.4	56.6
BRT-VP-3/14[b]	36.2	21.45	59.3	33.4	24.05	72.0	57.5
A. africanus							
N	5	5	4	8	7	4	7
Mean	33.6	20.4	64.4	32.8	21.2	64.4	49.7
SD	5.4	1.9	7.8	4.5	2.6	7.8	5.4
Range	27.2–40.0	18.8–23.6	53.2–70.1	26.4–37.3	17.8–25.0	53.2–70.1	40.2–55.2

[a] Definition follows Kimbel et al. (2004).
[b] Values are averaged from right and left sides.

between the hard palate and the nasoalveolar clivus, unlike most *A. afarensis* maxillae.

Differences between *A. afarensis* and *A. anamensis* are not well characterized yet, largely owing to the small sample size of *A. anamensis*. In the few *A. anamensis* specimens where features of the nasoalveolar region can be evaluated, morphology is generally similar to the typical *A. afarensis* pattern: the clivus is inclined, it extends well into the nasal aperture, and the nasal cavity is stepped (Ward et al., 2001; Haile-Selassie et al., 2019). However, the palate is deeper in the *A. anamensis* cranium (MRD-VP-1/1) than is typical of *A. afarensis*, both posteriorly and anteriorly (though the anterior depth of the MRD palate is distinct from the flexed palate of *A. africanus*). The clivus is insufficiently preserved in KNM-KP 29283 to make a precise assessment of anterior palate depth, although the KNM-ER 30745 palate is described as anteriorly shallow (Ward et al., 2001).

Both LDD maxillae exhibit the primitive configuration with regard to clivus and palate configuration: an intranasal platform is present, and the nasal cavity entrance is stepped (SOM Fig. S5). Both palates are shallow anteriorly. Depth increases posteriorly only moderately, and the LDD maxillae fall within one standard deviation of the *A. afarensis* mean with regard to palate depth at M^1/M^2 (Table 5). The inclination of the clivus has been quantified by the subnasal angle (Spoor et al., 2010). The clivus is not strongly inclined in the LDD maxillae, nor is it long. Together, these factors produce only moderate prognathism. An estimate of the subnasal angle in LDD-VP-1/126 is ca. 43–44°[1], which is slightly above the

Table 5
Measurements of the maxilla in LDD and comparative specimens. Comparative data from Kimbel et al. (2004), Ward et al. (1999, 2001), Haile-Selassie et al. (2019) and collected by the authors in this study. A list of comparative specimens is provided in SOM Table S2.

	Palate depth	Internal palate breadth			Palatal wedging[a]
	(M^1/M^2)	C^1	M^2	M^2/C^1	
LDD-VP-1/126	12.5	32.4	37.1	1.5	3.0
LDD-VP-1/248	11.4	33.5	38.6	1.2	9.1
BRT-VP-3/1	10.1	29.5	29.7	1.0	0.4
A. anamensis					
N	2	3	3	3	3
Mean	14.5	34.1	34.1	1.0	1.2
SD	4.2	0.38	0.46	0.02	3.1
Range	11.5–17.4	33.8–34.5	33.7–34.6	0.9–1.0	−1.4–4.6
A. afarensis					
N	6	7	7	7	7
Mean	11.3	28.2	32.1	1.1	7.0
SD	1.8	4.1	4.9	0.07	4.4
Range	8.5–14.0	23.1–35.0	25.0–41.0	1.0–1.2	−1.7–12.9
A. africanus					
N	3	2	2	2	3
Mean	16.2	27.5	32.9	1.2	10.2
SD	1.8	0.7	4.0	0.2	3.5
Range	14.5–18.0	27.0–28.0	30.0–35.7	1.0–1.3	6.4–13.4

[a] Definition follows Ward et al. (1999, 2001).

[1] Although prosthion is not preserved, its location can be estimated based on the orientation of the central incisor roots and the inferior extent of the fully preserved I^1/I^2 interdental septum.

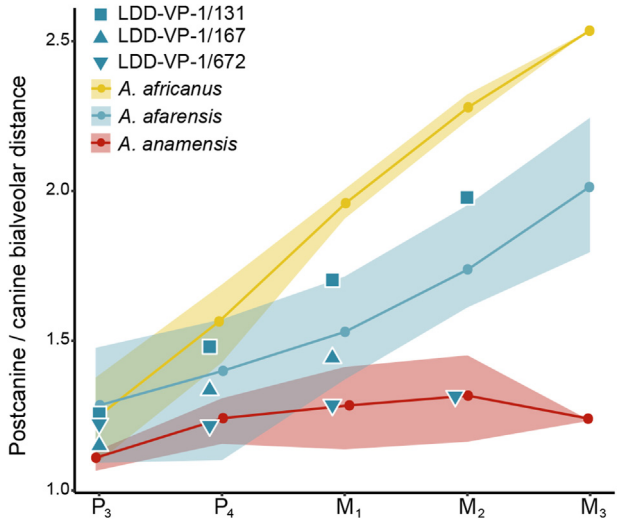

Figure 12. Mandibular arcade shape. The plot shows a ratio of postcanine to canine bialveolar margin distances, along the tooth row. Means (points and line) and ranges (fill) are shown for comparative species. The U-shaped arcade of *A. anamensis* is indicated by the comparatively flat line with ratio values just above 1, whereas the upward trending lines of *A. afarensis* and *A. africanus* reflect postcanine divergence. The LDD-VP-1/131 and LDD-VP-1/167 mandibles fall within or near the previously reported *A. afarensis* range, whereas LDD-VP-1/672 is more U-shaped. Comparative data from Kimbel et al. (2004) and supplemented by the authors in this study. A list of comparative specimens is provided in SOM Table S2.

range previously reported for *A. afarensis* (mean = 34.6°, SD = 3.5°, range 29–39°; see Spoor et al., 2010). The preserved portions of LDD-VP-1/248 suggest similar morphology, although the specimen is too damaged to estimate the subnasal angle.

Zygomatic root position The position of the zygomatic root played a role in the diagnoses of *K. platyops* and *A. deyiremeda*. The root of the zygomatic arises at the P^3/P^4 and P^4 level in these species (respectively), which is shifted anteriorly compared with *A. anamensis* and *A. afarensis* (Leakey et al., 2001; Spoor et al., 2010; Haile-Selassie et al., 2015). An anteriorly shifted zygomatic root is a feature that *K. platyops* and *A. deyiremeda* share with *Paranthropus*. Both LDD maxillae exhibit the primitive condition, with the zygomatic root positioned posteriorly.

Dental arcade shape *Australopithecus anamensis* possesses a primitive, U-shaped arcade. The canines are positioned nearly in-line with the premolars and molars, and there is minimal divergence in the molar row. In the mandible, the canine jugum extends further laterally than the premolar juga (Ward et al., 2001, 2020). In contrast, the canine is positioned more medially in *A. afarensis* and *A. africanus*, with greater postcanine divergence. Postcanine divergence has been quantified via measurement of internal bialveolar margin distances for the maxilla and mandible (Kimbel et al., 2004) as well as via the palatal wedging value (Ward et al., 1999, 2001).

Palate shape metrics demonstrate an increase in postcanine divergence across the *A. anamensis-A. afarensis- A. africanus* chronological series, indicating the evolutionary departure from the U-shaped arcade through time. The LDD maxillae exhibit moderate postcanine divergence. The palatal wedging metric shows that the LDD-VP-1/126 value falls within the region of overlap between *A. afarensis* and *A. anamensis*, whereas the value for LDD-VP-1/248 palate falls at the more divergent end of the *A. afarensis* range (Table 5).

For the mandible, bialveolar distance ratios show greatest overlap at the premolar level, and among-species differences become more pronounced in the molar row (Fig. 12; SOM Fig. S4). The degree of postcanine divergence varies among the LDD mandibles. The LDD-VP-1/131 arcade is the most divergent. Measurements were collected on the mirror-imaged reconstruction, but the divergence is easily observed on the original fossil, where the C_1 and P_3 roots are clearly positioned medial to the molar row. The reconstruction has a V-shaped arcade, similar to reconstructions of the considerably smaller specimen, A.L. 288-1. Compared with other early *Australopithecus* specimens for which internal bialveolar margin distances are possible to measure or estimate, LDD-VP-1/131 falls among the most strongly divergent mandibular arcades of *A. afarensis*, particularly similar to A.L. 444-2. Postcanine divergence in LDD-VP-1/167 is more gradual. Although the canine is positioned only slightly medial to the P_4-M_1 axis, divergence is clear in the original fossil because the entire external contour of the canine contributes to the anterior dental arc and the canine jugum lies medial to the premolar juga. Further, the relative positions of M_1 and M_2 roots suggest divergence within the molar row, though breakage prevents reliable measurement at the M_2 level. Bialveolar ratios from the LDD-VP-1/167 reconstruction fall near the *A. afarensis* mean. The postcanine dentition of LDD-VP-1/672, however, is minimally divergent. This specimen falls within the region of overlap for canine to premolar ratios, but within the *A. anamensis* range at the M_1 and M_2 levels.

The LDD-VP-1/131 and LDD-VP-1/672 specimens are reassembled from multiple fragments, which introduces a degree of uncertainty to the arcade shape reconstruction. However, mirror imaging across the preserved midline results in a smooth alveolar contour and results in overlap between the C_1–P_4 crowns or roots of one side and their mirror-imaged counterparts (Figs. 3H and 8B, D). This overlap after mirror imaging suggests that distortion about the arc of the anterior dentition and premolars is minimal.

An additional aspect of arcade shape relates to canine and incisor arrangement. In most species of non-robust australopith, the anterior teeth are arranged in an arch that is externally convex in the transverse plane. A diagnostic feature of *K. platyops* is the transversely flat arrangement of the canines and incisors (Leakey et al., 2001). The anterior teeth are arched in both LDD maxillae, with the anterior limit of the arch extending well beyond the bi-canine line.

Incisors The upper incisors of *A. afarensis* are described as possessing a pronounced basal tubercle and crowns that flare toward the incisal edge. These are thought to be primitive features, as basal tubercle expression is reduced in *A. africanus* incisors and crown edges more parallel (White et al., 1983). The LDD-VP-1/248 I^1 is very worn, but does not appear to possess a basal tubercle. Accordingly, the LaL dimension of this tooth is smaller than any other reported for *A. afarensis*, which is notable given that the other associated teeth demonstrate that this individual was not particularly small. The LDD-VP-1/248 I^1 is too worn and damaged to assess its MD dimensions or degree of crown flare. However, the I^2 shows a strongly flaring distal margin.

The differential diagnosis of *K. platyops* notes that the I^1 and I^2 roots are similarly sized in KNM-WT 40000 (Leakey et al., 2001). In LDD-VP-1/126 and LDD-VP-1/248, the I^1 root is large relative to the I^2 root, similar to other early species of *Australopithecus*.

Incisor wear has been described as lingually and distally angled for *A. afarensis* and *A. anamensis* (Johanson et al., 1982b; Ward et al., 2013). The LDD-VP-1/248 central incisor is somewhat different in having an occlusal wear surface that appears horizontally oriented both MD and LaL. The apparent lack of a distal slope to the wear plane is likely affected by the extreme wear state and preservation damage.

Canines The LDD sample includes one lower canine (LDD-VP-1/672) and antemeric upper canines (LDD-VP-1/248). These teeth are fragmentary and worn but still preserve diagnostic morphology.

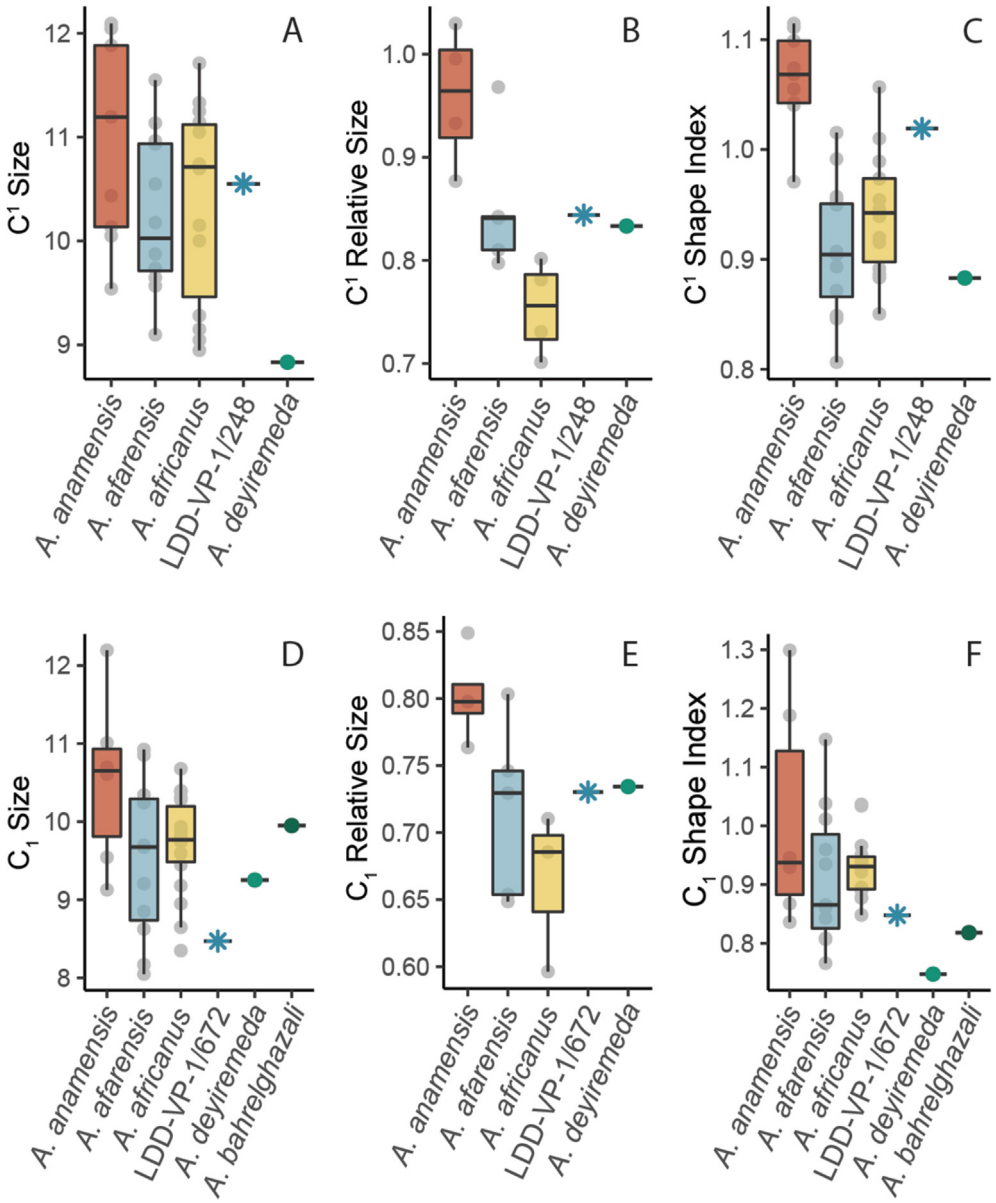

Figure 13. Quantitative comparison of upper (A–C) and lower (D–F) canines in early *Australopithecus* species. Absolute size (A, D) is the square root of the product of MD and BL basal dimensions, relative size (B, E) is normalized by M_1 or M^1 MD, and shape index (C, F) is MD divided by BL dimensions. LDD canine metrics are consistent with previously reported *A. afarensis* values. Values shown for LDD-VP-1/248 are averages of left and right sides. A list of comparative specimens is provided in SOM Table S2.

Comparing absolute size with other Pliocene hominin specimens (Fig. 13A, D) confirms that the LDD specimens represent small and large individuals. LDD-VP-1/248 falls among larger *A. afarensis* and *A. africanus* upper canines (similar in absolute size to A.L. 487-1, A.L. 333×-3 and A.L. 444-2). An absolutely small upper canine contributed to the diagnosis of *A. deyiremeda*, and LDD-VP-1/248 differs from BRT-VP-3/1 in this regard. The lower canine of LDD-VP-1/672 falls among the smallest *A. afarensis* and *A. africanus* lower canines (similar to A.L. 128-23 and A.L. 198-1).

Canine morphology has played a vital role in hominin systematics, with a strong focus on identifying primitive features in progressively older species. Trends from more primitive to more derived canine morphology include reduction in size, changes in basal tubercle or 'shoulder' height and a change in wear pattern. These morphological differences are related to the evolution of the incisiform canine and loss of the C^1–P_3 honing complex.

The evolutionary trend toward reduction in canine size is apparent when absolute canine size is normalized by a proxy of overall size (here, M_1 or M^1 MD). In both LDD specimens, relative canine size falls near the *A. afarensis* mean and outside the ranges of *A. anamensis* and *A. africanus* (Fig. 13B, E). The *A. anamensis* canine is MD elongated compared to later species, and the difference is especially pronounced in the upper canine (Manthi et al., 2012; Ward et al., 2013). The elevated shape index (MD/BL) of LDD-VP-1/248 falls within an area of overlap among early *Australopithecus* species, but more MD elongated than is typical of *A. afarensis*

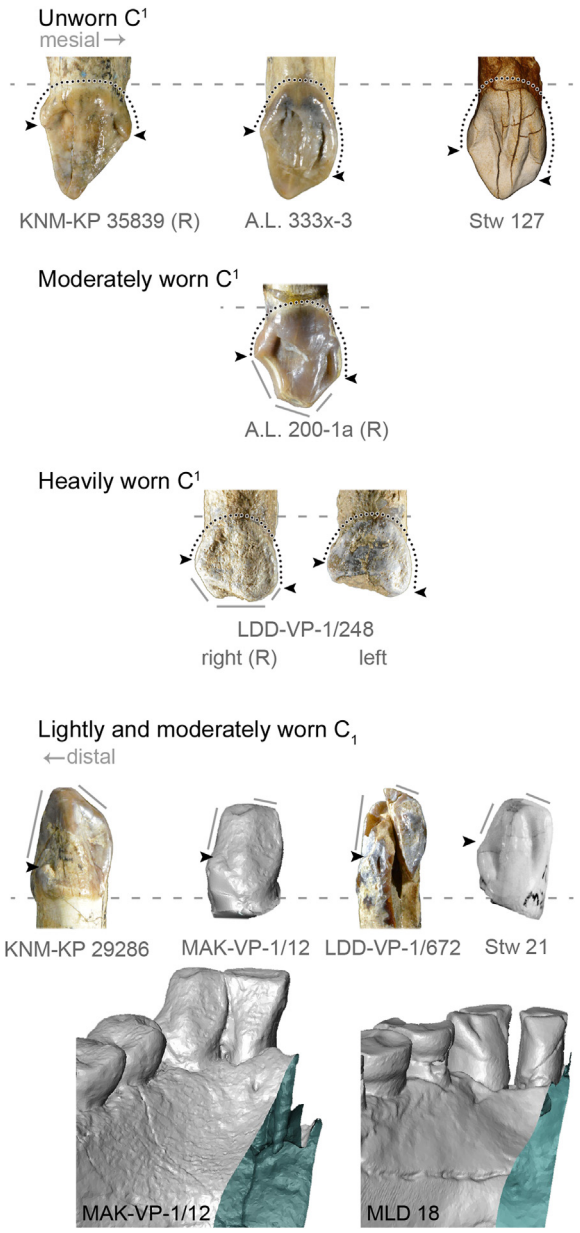

Figure 14. Qualitative canine features in *A. anamensis* (KNM-KP 35839, KNM-KP 29286), *A. afarensis* (A.L. 333×-3, A.L. 200-1a, MAK-VP-1/12), *A. africanus* (Stw 127, Stw 21) and LDD specimens. Black arrowheads indicate the height of the mesial and distal tubercles (or 'shoulders'). In both upper and lower canines, the tubercles shift apically across chronologically progressive species. As a result, the canine tip becomes less projecting. Black dotted lines on the upper canines parallel the tubercles and the gingival eminence. Although the LDD-VP-1/248 upper canines are worn, it is clear that they possess the *A. afarensis* pattern: the mesial shoulder is upright and extends past mid-crown, whereas the distal tubercle is low and distally projecting (note that mesial shoulder height in LDD-VP-1/248 canines are affected by wear). Solid grey lines parallel wear facets on *A. afarensis* upper canines. The heavily worn LDD-VP-1/248 right canine presents apical, distolingual and mesial wear facets, similar to A.L. 200-1a. On lower canines, solid grey lines indicate the length and orientation of the occlusal crests. As tubercles shift apically, the occlusal crests become shorter and less steeply inclined. The LDD-VP-1/672 lower canine has a short and sub-horizontal mesial occlusal crest combined with a long and steep distal occlusal crest, similar to other *A. afarensis* specimens. The MAK-VP-1/12 lower canine is shown in the dental row to illustrate how the differences in occlusal crest length and orientation relate to the 'canine step' pattern, which is not present in *A. africanus*. All specimens are scaled to the same crown height (estimated in worn specimens), aligned at the cervix (grey dashed line) and shown as lefts (R indicates reversed images). Image of Stw 21 kindly provided by J. Moggi-Cecchi and Images of KNM-KP 35839 and KNM-KP 29286 © National Museums of Kenya.

(Fig. 13C). *Australopithecus afarensis* specimens with similar C^1 shape indices include L.H. 6[2] and KNM-RK 53800 (Mbua et al., 2016).

Qualitative features of the LDD canines are also most similar to *A. afarensis*. In this species, upper canines tend to exhibit a mesial shoulder that is upright and extends toward the crown tip (well beyond mid-crown height). Due to the upright orientation of the mesial shoulder, the crown margins connect via the gingival eminence in a roughly U-shaped contour (Fig. 14). Although the LDD-VP-1/248 C^1s are worn, the mesial margin clearly has an upright orientation and the shoulder would have extended well beyond mid-crown height when unworn. These teeth are morphologically quite similar to A.L. 333×-3, despite the marked difference in wear states. In contrast, both mesial and distal basal tubercles of *A. anamensis* are similarly short and splay outward (Ward et al., 2001; also see; Haile-Selassie et al., 2019). These structures follow a more open, parabolic course that contributes to the symmetrical, diamond-shaped outline of the upper canine crown in this species.

Differences in lower canine morphology are less marked, but still informative. The distal tubercle is shortest in *A. anamensis* and extends slightly more apically in *A. afarensis* and *A. africanus* (Fig. 14). In LDD-VP-1/672, the distal tubercle is set low on the crown, but not as low as seen in the Kanapoi C_1s KNM-KP 47953, KNM-KP 29284, and KNM-KP 29286. The distal tubercle is also slightly lingually positioned in LDD-VP-1/672, which is a feature shared with a number of *A. anamensis* and *A. afarensis* specimens. This feature is best seen in occlusal view, where the arc distance from the mesial to distal tubercle is shorter about the circumference of the lingual face than it is about the labial face. In contrast, *A. africanus* lower canines tend to have the mesial and distal shoulders positioned directly opposite each other. The overall morphological pattern of the LDD-VP-1/672 canine is a good match to A.L. 198-1.

Between-species differences in canine wear pattern have also been documented. *Australopithecus anamensis* upper canines are described as combining both apical and distally sloping wear facets (Ward et al., 2001). However, the distally sloping facet on the lingual surface is the most pronounced at intermediate and later wear stages in *A. anamensis* (e.g., ASI-VP-2/2, MRD-VP-1/1 and KNM-KP 58309). In *A. afarensis*, the intermediate wear stage is characterized by primarily horizontal apical wear, with additional mesial and distolingual extensions (A.L. 200-1a). Upper canines of *A. africanus*, in contrast, tend toward more horizontal apical wear (White et al., 1983). The less worn right C^1 of LDD-VP-1/248 exhibits the *A. afarensis* wear pattern: primarily horizontal but with a clear mesial and distolingual extension present (Fig. 14).

Recent discoveries have led to the recognition that a long and large canine root distinguishes *A. anamensis* from *A. afarensis* (Manthi et al., 2012; Ward et al., 2013). The LDD-VP-1/672 root is absolutely short. At 17.5 mm, it falls below the previously reported minimum for *A. afarensis* (Manthi et al., 2012; Ward et al., 2013). Although portions of the root are missing, it is clear that the root's cervical area falls among the smaller *A. afarensis* specimens, which would indicate a similarly small root volume. Average root length of the LDD-VP-1/248 canines is 23.6 mm, roughly at the previously reported *A. afarensis* average (mean = 23.0, SD = 4.0, range = 18.8–28.1; data from Manthi et al., 2012 and Ward et al., 2013).

[2] The distal tubercle of L.H. 6 is damaged and the MD dimension estimated. Here, we use an estimated MD dimension of 10 mm, less than the 10.1+ mm figure reported by White (1977). The values reported here for L.H. 6 can be considered a minimum estimate of MD elongation.

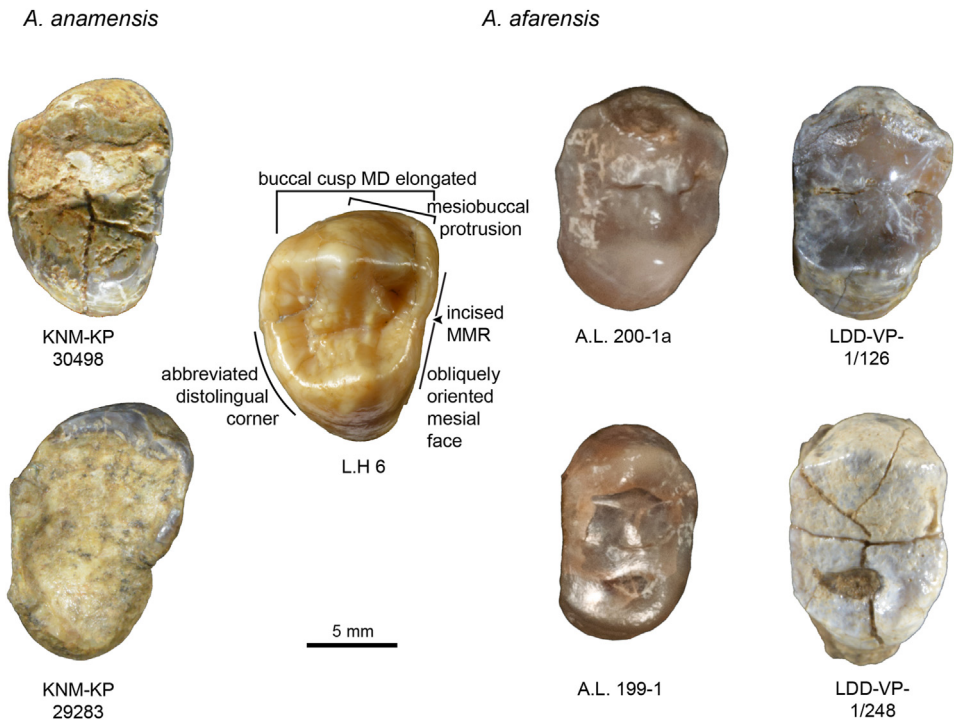

Figure 15. Qualitative P^3 features in *A. anamensis, A. afarensis* and LDD specimens. Primitive features are annotated on L.H. 6 (and also present in *A. anamensis* specimens). The LDD P^3s are similar to the more derived Hadar specimens with respect to their well-defined distolingual corners, reduced mesiobuccal protrusion and rectangular occlusal fovea, resulting from similarly elongated buccal and lingual cusps and mesial face oriented roughly perpendicular to the axis of the paracone crests. Images of A.L. 200-1a and A.L. 199-1 kindly provided by W.H. Kimbel, images of KNM-KP 30498 and KNM-KP 29283 © National Museums of Kenya.

Upper premolars Upper premolars are thought to be less informative than their counterparts in the lower jaw (Wood and Abbott, 1983; Wood et al., 1983; Wood and Uytterschaut, 1987; Wood and Engleman, 1988), but they nonetheless present some phylogenetically and taxonomically informative morphology. Previous research described how P^3 form in *A. afarensis* is more primitive than in *A. africanus*. Primitive features include: (in occlusal view) a mesiobuccal protrusion of the crown, an obliquely oriented mesial face, an abbreviated distolingual crown corner, a MD elongated paracone, and the presence of a groove incising the Mmr and continuing onto the mesial face (Remane, 1954; Şenyürek, 1955; White et al., 1983; Suwa, 1990). These features give the crown an asymmetric outline and a triangular occlusal fovea (Fig. 15).

Studies describing the primitive nature of *A. afarensis* P^3s were based largely on the Laetoli sample (Garusi 1: Remane, 1954; Şenyürek, 1955 and L.H. 6: Suwa, 1990). The Hadar collection from the 1970's includes only two P^3s that are complete and lightly worn enough to preserve clear occlusal morphology (A.L. 200-1a and AL 199-1). Suwa (1990) noted that although the primitive features described above were often used to characterize *A. afarensis* as a species, they more accurately describe the older Laetoli sample. The Hadar sample, in contrast, lacks many of these features. In fact, Suwa (1990) identified P^3 morphology as one of the largest dental differences between the Laetoli and Hadar samples. As the fossil record has expanded, it has become more apparent that these primitive features of the P^3 are even more pronounced in *A. anamensis* (Fig. 15). Thus, the morphology of this tooth also shows a temporal trend in the *A. anamensis-A. afarensis* lineage.

The LDD P^3s are quite similar to each other (despite differing in wear stage) and show a clear affinity to the Hadar *A. afarensis* sample. Both of these specimens have a symmetrical outline and rectangular occlusal fovea (in occlusal view): the mesiobuccal protrusion is weak or absent, the paracone and protocone crests are of similar MD lengths, the mesial face is perpendicular to the MD axis and distolingual corner is angular and well defined. The LDD-VP-1/126 P^3 does show a groove incising the Mmr, which may not sort as neatly along the temporal trend as the other features listed above.

Other aspects of P^3 morphology further ally the LDD specimens with *A. afarensis*. In lingual view, the wear of the protocone is strongly angled and asymmetric, with a short mesial crest separated from a longer and more sharply inclined distal crest (Fig. 6). This angled and asymmetric wear pattern distinguishes *A. afarensis* from *A. africanus* and subsequent species (White et al., 1983; Suwa, 1990). The cusps also lack the inflated appearance described for some *A. africanus* and *Paranthropus robustus* specimens (White et al., 1983; Suwa, 1990; Moggi-Cecchi et al., 2006). In mesial view, the buccal and lingual walls of the LDD P^3s are vertically oriented and lack the strong sloping described for Garusi 1 and associated with *A. anamensis* cheek teeth.

Taxonomically relevant features of the P^4 include the presence/absence of buccal grooves, a distolingual pit, a distobuccal cuspule, and other accessory cuspules on the Dmr. These features have primarily been described as useful in distinguishing robust from non-robust australopiths, but they have also been referenced in comparisons of *A. africanus* and *A. afarensis* (Suwa, 1990; Moggi-Cecchi et al., 2006). Suwa (1990) found that a distolingual pit occurs commonly in *P. robustus*, less commonly in *A. africanus*, but only in one *A. afarensis* P^4. The LDD-VP-1/126 P^4 exhibits a distolingual pit, formed by an accessory ridge that runs distobuccally from the Pr to the Dmr. It also exhibits a deep distal buccal groove and a distal lingual groove—features that occur more commonly in *A. africanus* or robust australopiths, but are documented at low frequency in the previously known *A. afarensis* sample (Suwa, 1990; Moggi-Cecchi et al., 2006).

Lower premolars Morphology of the P_3 is particularly informative with regard to early *Australopithecus* systematics, because a

number of features are expressed in a more derived state in progressively younger species. In *A. anamensis*, the P_3 protoconid lies near the center of the crown due to the sloping buccal face. The metaconid is poorly developed, such that the tooth is described as unicuspid (Delezene and Kimbel, 2011) or nearly so (Ward et al., 2001). The longitudinal groove is absent. Internal crown structures are arranged such that a line connecting the mesial and distal protoconid crests is oriented mesiolingual-distobuccally, and the transverse crest angles distally. As a result, the anterior and posterior fovea are nearly the same size. Further, the mesial marginal ridge is set low on the crown and, in occlusal view, the mesial and lingual segments of this ridge are not continuous—creating the open anterior fovea (Ward et al., 2001; Kimbel et al., 2006; Delezene and Kimbel, 2011).

In the comparatively derived *A. africanus* P_3, the buccal face is upright, which positions the protoconid close to the buccal margin. The metaconid is large. The transverse crest is roughly perpendicular to the protoconid crests and divides a small anterior fovea from a relatively large posterior fovea. A longitudinal groove often bisects the transverse crest. The tooth's mesiodistal axis parallels the protoconid crests. The crests and ridges of the crown are thick and the basal outline of the crown is round and symmetrical.

The *A. afarensis* P_3 is highly variable, with some specimens exhibiting crown morphology closer to the *A. anamensis* pattern and others closer to the *A. africanus* pattern. This variation has been described as 'phylogenetic polymorphism', in which a conspecific sample exhibits a mixture of primitive and derived states for a given feature, reflecting the phylogenetically intermediate position between an ancestor that is uniformly primitive and a descendent species that is uniformly derived (Kimbel et al., 2004; Delezene and Kimbel, 2011).

The LDD-VP-1/672 P_3 falls toward the primitive end of the *A. afarensis* range of variation. The crown has an asymmetric outline and the anterior fovea is somewhat open. No longitudinal groove is present. An additional primitive feature in this specimen is the presence of a contact facet on the buccal face of the P_3 (Fig. 9, inset), which constitutes a vestigial remnant of the C^1—P_3 honing complex. However, the LDD-VP-1/672 P_3 also presents a number of derived features that distinguish it from the *A. anamensis* pattern and clearly indicate affinity with *A. afarensis*: the protoconid is buccally placed, the metaconid is fairly well-developed, the protoconid crests are parallel to the crown's mesiodistal axis, the mesial marginal ridge is positioned high on the crown, the transverse crest is BL oriented, and the posterior fovea is relatively large. The mix of primitive and derived features present in the LDD-VP-1/672 P_3 can be matched by Hadar specimens A.L. 128-23 and A.L. 198-1.

Metrics for the LDD-VP-1/672 P_3 (following the methods of Delezene and Kimbel, 2011) are reported in SOM Table S3. Delezene and Kimbel (2011) showed that *A. afarensis* and *A. anamensis* samples are statistically distinguishable with respect to the orientation of the protoconid crests, the relative size of the posterior fovea, and mesial crown breadth. The LDD-VP-1/672 P_3 falls in regions of overlap between *A. afarensis* and *A. anamensis* with regard to protoconid crest orientation and mesial crown breadth, but possesses a distinctly expanded posterior fovea, like other *A. afarensis* specimens. Both occlusal area (SOM Table S3) and traditional caliper measurements show that the LDD-VP-1/672 P_3 is small (Fig. 16A).

Previous comparisons among early *Australopithecus* species have revealed primitive to derived trends in the P_4 as well. However, the magnitude of intraspecific variation is large and interspecific overlap is extensive. Despite this overlap, the LDD-VP-1/672 P_4 nonetheless possesses some features indicating a strong affinity to *A. afarensis* and outside the range of *A. anamensis*. The *A. anamensis* P_4 tends to have an ovoid basal outline that is BL broad relative to MD length. Further, the cusps are centrally placed, so that the trigonid and talonid are similarly sized (Ward et al., 2001, 2020). The LDD-VP-1/672 P_4 is similar to those of *A. afarensis*, *A. africanus* and KNM-WT 8556 in being quite MD elongated (Fig. 16F). The cusps are also mesially placed and the talonid is relatively large (Haile-Selassie and Melillo, 2015; Ward et al., 2020). The LDD-VP-1/672 P_4 crown possesses a distally projecting distolingual corner and abbreviated distobuccal corner. Such an outline distinguishes *A. afarensis* P_4s from other early *Australopithecus* species (White et al., 1983; Suwa, 1990; Haile-Selassie and Melillo, 2015). This tooth is a close match to A.L. 207-13 and A.L. 400-1a with regard to the crown outline and cusp pattern (i.e., all specimens present a distinct End and Hyd, well-defined lingual transverse groove with a distally projecting extension, and lack cuspules on the Dmr).

Molars Molar morphology overlaps extensively among early australopiths. This overlap is greatest between *A. anamensis* and *A. afarensis*, whereas a small number of features distinguish *A. africanus, A. deyiremeda,* and *K. platyops* and associated specimens from Lomekwi, Kenya.

Small and BL narrow upper molars were listed as distinguishing features of *A. deyiremeda* and *K. platyops* (Leakey et al., 2001; Haile-Selassie et al., 2015). The LDD sample includes only two upper molars: the LDD-VP-1/126 M^2 and the heavily worn LDD-VP-1/775 (the latter specimen was recovered as an isolated tooth and could be either an M^1 or M^2). The LDD upper molar dimensions fall comfortably within the *A. afarensis* range of variation and do not share the small size of *A. deyiremeda* and *K. platyops*.

Australopithecus africanus lower molars tend to be larger, on average, than other non-robust species, and the M_1 slightly more elongated (White et al., 1983; Suwa et al., 1994). Most of the recently published lower molars from Lomekwi overlap with *A. anamensis* and *A. afarensis* in MD and BL dimensions, although a high incidence of well-developed protostylids and accessory cuspules are described as distinguishing features of that sample (Skinner et al., 2020).

The LDD lower molar sample exhibits a moderate incidence of cingular remnants and accessory cusps. Out of six specimens where the morphology can be assessed, a protostylid is well-developed in only one specimen (LDD-VP-1/732), clearly present in a second (LDD-VP-1/167), and ambiguous in a third (LDD-VP-1/764). The common accessory cusps occur with moderate frequency, but development of additional accessory cuspules is limited. Size and shape of the Woranso-Mille EEA lower molars generally fall within the extensively overlapping *A. afarensis* and *A. anamensis* ranges of variation. LDD-VP-1/167, LDD-VP-1/672 and LDD-VP-1/1065 fall among the smaller comparative specimens, whereas teeth from the previously described NFR-VP-1/29 mandible fall among the largest. Those from the *A. deyiremeda* mandible (BRT-VP-3/14) are intermediate (Fig. 17). The single exception, however, is the LDD-VP-1/406 M_3.

The LDD-VP-1/406 specimen falls more than three standard deviations below the *A. afarensis* mean, regardless of whether crown size is measured as area (SOM Table S4) or by caliper measurements (Fig. 17). Aside from the small size, the LDD-VP-1/406 crown exhibits typical features of non-robust australopiths: the crown is bunodont, the buccal cusps are flattened by wear, whereas the lingual cusps maintain relief and the crown outline tapers distally. A CT scan reveals thick enamel (Fig. 7). The protoconid is too worn to reconstruct relative enamel thickness for the entire crown, but average enamel thickness for the lingual portion of the enamel cap is similar to values reported for other non-robust australopith molars (LDD-VP-1/406: ca. 1.3, *A. anamensis*: mean = 1.11, SD = 0.15; *A. afarensis*: mean = 1.36, SD = 0.13; *A. africanus*: mean =

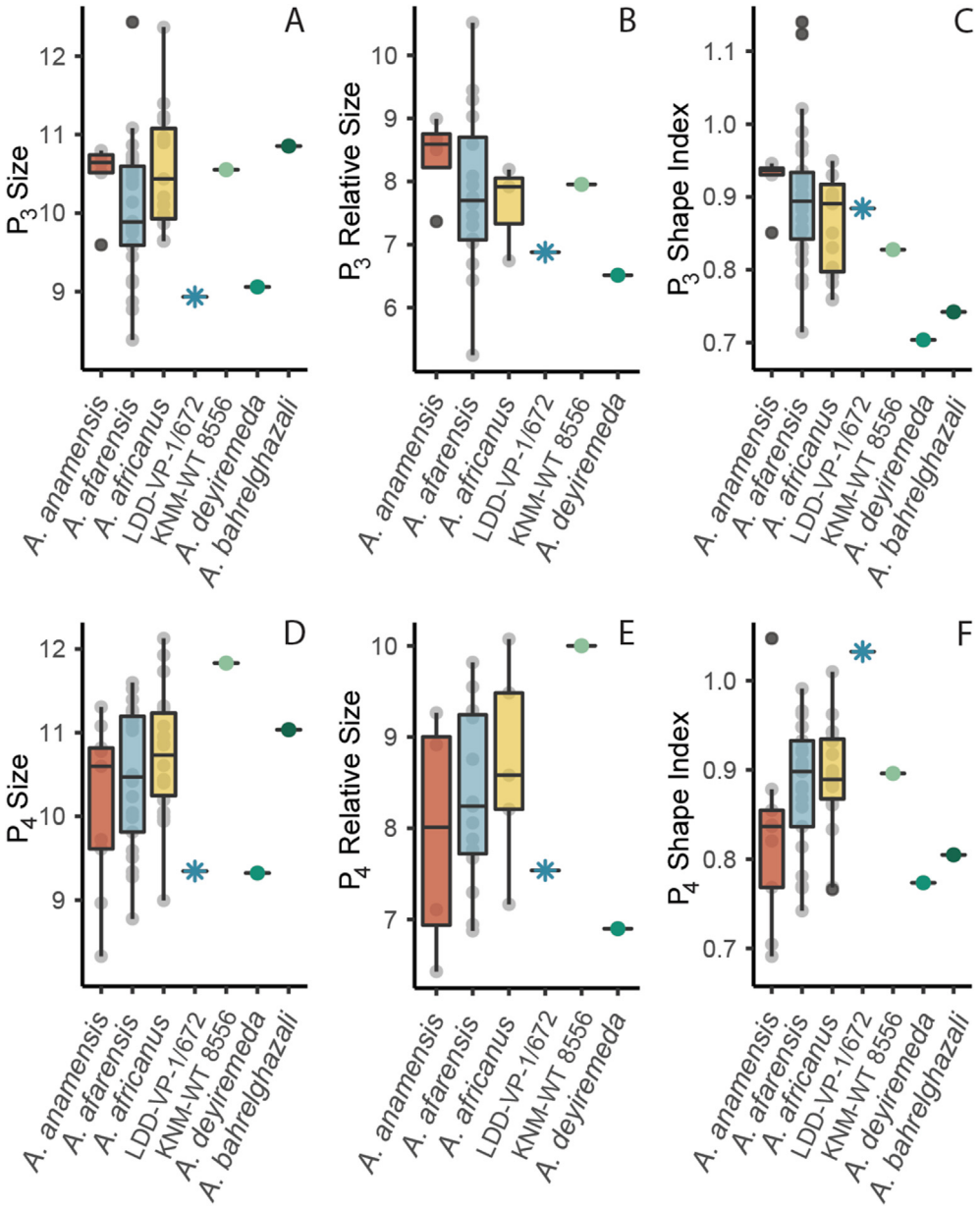

Figure 16. Quantitative comparison of P_3 (A–C) and P_4 (D–F) in early *Australopithecus* species. Absolute size (A, D) is the square root of the product of MD and BL basal dimensions, relative size (B, E) is normalized by M_1 or M^1 MD, and shape index (C, F) is MD divided by BL dimensions. Values show that LDD-VP-1/672 represents an absolutely small individual, with relative size and shape falling in regions of overlap between *A. afarensis* and *A. africanus*. Note the large magnitude of variation in *A. afarensis* P_3 values. The *A. afarensis* outlier in (A) is DIK-2-1. A list of comparative specimens is provided in SOM Table S2.

1.50, SD = 0.21; methods and comparative data from Skinner et al., 2015). The only additional morphological features of note for LDD-VP-1/406 are that the buccal cusps occupy most of the crown area (due to the lingual position of the longitudinal groove) and the Prd and Hld are particularly large (SOM Table S4). Although relative cusp size has not been reported for *A. anamensis*, molars in the holotype mandible (KNM–KP 29281) also show a lingually positioned longitudinal groove and relatively large buccal cusps (Ward et al., 2001), though not to the same degree as LDD-VP-1/406.

LDD-VP-1/406 is most similar in size to a comparably small M_3 recently reported from Lomekwi, KNM-WT 38347 (Skinner et al., 2020). In addition to the similarity in size, both specimens lack a distal fovea. However, they display different cusp patterns. LDD-VP-1/406 lacks a C6 and possesses a C7, whereas the inverse is true of KNM-WT 38347. The lingually positioned longitudinal groove and relatively large buccal cusps that characterize the LDD-VP-1/406 crown are not present in KNM-WT 38347. Cusp pattern is polymorphic in early *Australopithecus* species, and the differences between these two specimens fall within the previously documented range of variation.

KNM-WT 38347 is identified as an M_3 (or possibly M_2). The small size of the specimen is described as "extremely aberrant" (Skinner et al., 2020: 11), leading the authors to discuss the possibility that the tooth represents a supernumerary molar. We identify LDD-VP-1/406 as an M_3 based on the MD elongated crown outline, BL narrow talonid and lack of a distal IPCF (despite being in full occlusion and considerably worn). We cannot rule out the possibilities that the specimen represents an M_4 or an idiosyncratically small outlier, but we do not favor these explanations. First, although supernumerary molars occur rarely in extant and fossil hominoids (Johanson et al., 1982b; Schwartz, 1984), they exhibit a high frequency of malformation and the nature of the

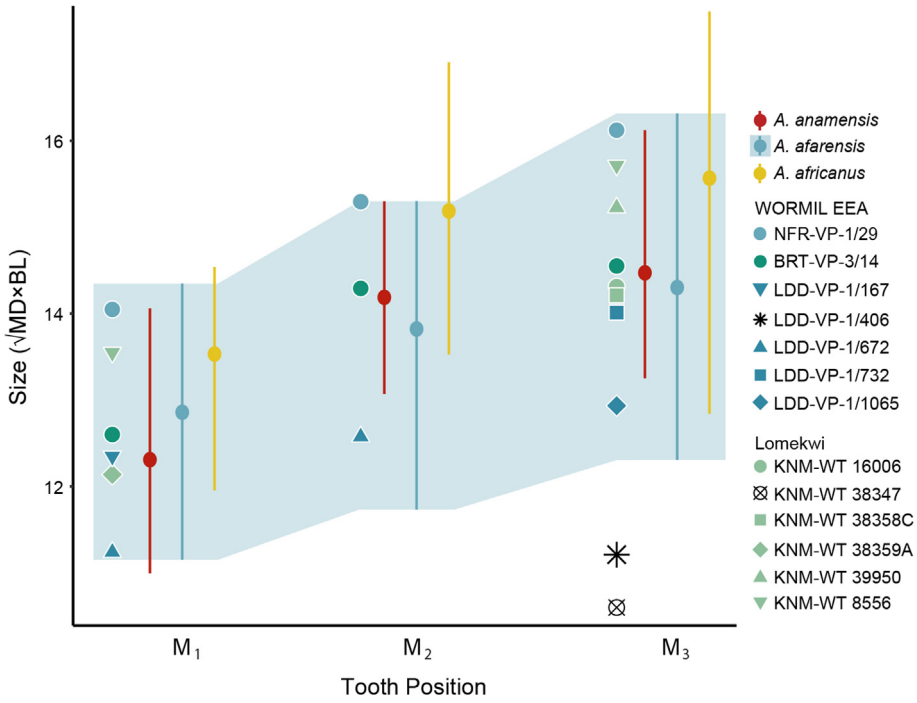

Figure 17. Molar size in early *Australopithecus* species. Points with associated bars indicate means and ranges. The blue fill delimits the *A. afarensis* range. Specimens from the Woranso-Mille EEA localities (plotted to the left of the comparative data) show a moderate increase in size with more distal tooth position, consistent with early *Australopithecus* species. The EEA specimens span most of the *A. afarensis* range, with the exception of the very small LDD-VP-1/406 M_3, which is similar in size to KNM-WT 38347. A list of comparative specimens is provided in SOM Table S2. (For interpretation of the references to color in this figure legend, the reader is referred to the Web version of this article.)

malformations is inconsistent. However, neither LDD-VP-1/406 nor KNM-WT 38347 exhibits morphology that appears developmentally abnormal and both specimens depart from typical *Australopithecus* M_3s in the same direction and to a similar degree. Second, there are now two instances of this morphology documented within a similar period, and the repeated observation disfavors the hypothesis that both teeth represent developmental anomalies or idiosyncratic outliers. While additional fossil material is needed to ultimately resolve this issue, an alternative to the developmental anomaly and outlier hypotheses is that the size variation represents taxonomic heterogeneity. In this context, it is notable that small dental size played a role in the diagnoses of both *K. platyops* from Lomekwi and *A. deyiremeda* from the EEA of Woranso-Mille. The taxonomic implications of variation in M_3 size in the 3.5–3.2 Ma Woranso-Mille sample are discussed further below.

4. Discussion

4.1. Taxonomic attribution

The more complete specimens from LDD can be securely attributed to *A. afarensis*. With regard to the LDD mandibles (LDD-VP-1/131, LDD-VP-1/167 and LDD-VP-1/672), cross-sectional corpus contours fall within the previously documented range of *A. afarensis*. They do not exhibit features related to the receding symphysis that characterizes *A. anamensis*, nor do they exhibit the features of the lingual aspect of the symphysis distinctive in *A. bahrelghazali*. Corpus size and shape at more distal positions are also consistent with assignment to *A. afarensis*. The LDD mandibles do not possess the anteriorly positioned ramus root and broad corpus referenced in the *A. deyiremeda* diagnosis, nor the shallow and inflated corpus typical of *A. africanus*. Like other *A. afarensis* mandibles, preserved morphology of LDD specimens suggest a low position of the mental foramen, high position for the ramus root, narrow extramolar sulcus and everted base.

The dentition of LDD-VP-1/672 presents a number of features diagnostic of *A. afarensis*. The C_1, P_3 and P_4 each present a combination of features that is more derived than typical of *A. anamensis*, more primitive than *A. africanus*, and distinct from the unusual premolar morphology of KNM-WT 8556. Relative shoulder height and wear pattern of the LDD-VP-1/672 C_1 suggests the presence of the canine step. Relative size and shape of the canine and premolars fall near *A. afarensis* means.

With regard to the maxilla, LDD specimens (LDD-VP-1/126 and LDD-VP-1/248) exhibit the primitive configuration of a stepped nasal cavity, and possess an intranasal platform and a shallow palate. These specimens are further similar to *A. afarensis* with regard to their moderately divergent tooth rows (consistent with arcade shape in mandibles LDD-VP-1/131 and LDD-VP-1/167). The zygomatic root is posteriorly positioned in the LDD maxillae, unlike in KNM-WT 40000 (*K. platyops*) and BRT-VP-3/1 (*A. deyiremeda*). The LDD P^3s are specifically similar to Hadar *A. afarensis* with regard to their symmetry, well-defined corners and rectangular occlusal fovea. Morphology of the LDD-VP-1/248 C^1 (shoulder height and orientation, relative size and wear pattern) is also consistent with an *A. afarensis* attribution.

The only features present in the LDD maxillae, mandibles and associated dentitions that depart from the 'classic' *A. afarensis* pattern are the absence of a clearly defined lateral corpus hollow in LDD-VP-1/167, the U-shaped dental arcade of LDD-VP-1/672, the mesiodistal elongation of the LDD-VP-1/248 C^1, the absence of the spinal crest and sharp inferolateral corner delimiting the nasal aperture in LDD-VP-1/126, and less pronounced subnasal prognathism. However, these differences are balanced against the numerous features listed above that indicate affinity to *A. afarensis*—and specifically to the Hadar site sample. Further, none of the features diagnostic of other middle Pliocene species (i.e., *A. bahrelghazali*, *K. platyops*, *A. deyiremeda*) are expressed in the LDD sample. The isolated molars from LDD are consistent with an *A. afarensis* attribution in terms of their crown dimensions, bilobate

contours and moderate frequency of accessory cusps and cingular remnants. We therefore also attribute the LDD isolated molars to *A. afarensis*, with the exception of LDD-VP-1/406, which we leave unassigned.

4.2. Morphological variation and temporal trends in *Australopithecus afarensis*

Our characterization of *A. afarensis* morphology is heavily influenced by fossils from Hadar because this site sample comprises the majority of the hypodigm. Additional specimens securely or provisionally attributed to *A. afarensis* (i.e., those from Laetoli, Dikika, Maka, and, depending on one's taxonomic inclinations, from Omo, Koobi Fora, West Turkana and Chad) depart from Hadar *A. afarensis* morphology in various ways. Such differences are usually attributed to temporal or geographic factors because these fossils derive from different spatiotemporal contexts.

Specimens from LDD-VP-1 sample the period from 3.41 to >3.33 Ma, similar in age to the Maka Sands (at Middle Awash) and the Basal through lower Sidi Hakoma Members of the Hadar Formation (at Hadar and Dikika). During this period, sample sizes are small compared to younger intervals of the Hadar Formation. Because small sample sizes are associated with an elevated risk of sampling error, morphology of the older Ethiopian *A. afarensis* sample is not well characterized (particularly for the maxilla). Studies of *A. afarensis* temporal trends rely on the inclusion of samples from elsewhere to represent earliest *A. afarensis*, making it difficult to disentangle temporal, geographic and stochastic (population-level) sources of variation. One important aspect of the LDD fossils is that they contribute to increasing sample size at ca. 3.4 Ma, without substantially increasing geographic variation.

The LDD sample falls within the previously documented range of variation of the Ethiopian *A. afarensis* sample in most aspects of morphology. Only a few features fall outside that range—namely measurements of mandibular arcade shape and subnasal prognathism. With regard to arcade shape, the expansion in variation is more an artifact of preservation than a case of the LDD specimens actually introducing new morphological variants into the hypodigm. Available data on *A. afarensis* arcade shape (Kimbel et al., 2004) come from a subset of mandibles that are well-preserved enough to be measured via mirror-imaging, but do not capture the entire range apparent from qualitative consideration of the full sample (Kimbel and Delezene, 2009). More advanced reconstruction methods and quantitative treatment of variation in *A. afarensis* mandibular arcade shape is needed. Available data on subnasal clivus angle (Spoor et al., 2010) may be similarly affected. Moreover, the maxilla sample is comparatively small.

The LDD sample does, however, increase the frequency of morphological variants that were previously documented in only one or very few specimens. For instance, the presence of a lateral corpus hollow is recognized as a diagnostic feature of the *A. afarensis* mandible (Johanson et al., 1978; White et al., 2000; Kimbel and Delezene, 2009) and the lack of this feature is listed as one of the distinguishing characteristics of the *A. deyiremeda* mandible (Haile-Selassie et al., 2015). The presence or absence of the hollow has thus played an important role in early *Australopithecus* taxonomy, but its development appears to be more variable than previously appreciated. Both the DIK-2-1 (Alemseged et al., 2005) and LDD-VP-1/167 mandibles depart from classic *A. afarensis* morphology in lacking the structures that traditionally define the hollow. The lateral prominence is absent or poorly developed in both specimens and a depression posterior to the mental foramen is absent in LDD-VP-1/167 and described as having an atypical form in DIK-2-1 (Alemseged et al., 2005). However, specimens with a characteristic hollow have been recovered from comparably old strata at Maka (White et al., 2000) and older strata at Laetoli (White, 1977), so it is unclear whether the variation in this feature is related to geological age.

Only one *A. afarensis* upper canine (L.H. 6) in the previously known sample is MD elongated to a similar degree as *A. anamensis* upper canines and the temporal component of this variation has been discussed previously (Kimbel et al., 2006). Dated to 3.7–3.6 Ma, L.H. 6 is among the older representatives of *A. afarensis* (Deino, 2011; Ditchfield and Harrison, 2011; Harrison, 2011). LDD-VP-1/248 constitutes a considerably younger fossil showing similarly elongated basal dimensions, but these dimensions appear in combination with qualitative crown structures that are more derived (i.e., Hadar-like) than those seen in L.H. 6. Another specimen exhibiting a fair degree of MD elongation in combination with derived qualitative features is the upper canine from Kantis, Kenya, KNM-RK 53800 (shape index = 0.99; Mbua et al., 2016). Like LDD-VP-1/248, KNM-RK 53800 is dated to chron C2An.3n (3.59–3.33 Ma).

A number of additional temporal trends have been identified in the *A. afarensis* or combined *A. anamensis* + *A. afarensis* hypodigms. This work has been important in documenting the evolutionary loss of the C^1–P_3 honing complex and establishment of masticatory robusticity in *Australopithecus* (Lockwood et al., 2000; Kimbel et al., 2006). The presence and robustness of such trends benefit from re-evaluation as new specimens are discovered from poorly sampled periods.

Building on the work of Lockwood et al. (2000), Delezene and Kimbel (2011) found that the currently available sample of *A. afarensis* P_3s shows a significant reduction in MD length over time, associated with a change in shape (such that crowns become BL broader, relative to MD length). The main driver of these trends appears to stem from differences between the Laetoli and Hadar samples. The new LDD-VP-1/672 P_3 falls between the two Hadar specimens of similar age (i.e., A.L. 198-1 and A.L. 128-23) in both MD length and shape index, which strengthens previous observations for this time interval.

Lockwood et al. (2000) also found evidence of a reduction in P_3 crown size over time. However, this trend was no longer present in the dataset of Delezene and Kimbel (2011), which included more recently recovered large P_3s from the youngest intervals—observations that countered the size reduction trend. The LDD sample also counters the size reduction trend, but does so in the inverse manner: the LDD-VP-1/672 P_3 contributes a very small P_3 to one of the older intervals. Indeed, the vast majority of variation in P_3 size is accounted for by specimens from the older half of the *A. afarensis* chronological range. This includes the largest *A. afarensis* P_3, DIK-2-1, dated to >3.4 Ma, and very small P_3s from LDD-VP-1/672 and A.L. 128-23 dated to ca. 3.4–3.33 Ma. It is further notable that the marginally younger NFR-VP-1/29 mandible (ca. 3.3 Ma) preserves the roots of what was likely a very large P_3. Delezene and Kimbel (2011) previously noted that P_3 size is significantly more variable in the *A. afarensis* hypodigm than in a comparative *Pan* sample, and near the significance threshold compared to a *Gorilla* sample. Specimens from the EEA at Woranso-Mille provide evidence that most of this variation is observed within a tightly constrained spatiotemporal window.

Lockwood and colleagues also observed an increase in mandible corpus size over time. The DIK-2-1 and NFR-VP-1/29 mandibles do not fall neatly into that trend because they are both very large and come from the chronologically older to intermediate intervals of the *A. afarensis* sample. However, Haile-Selassie et al. (2016a) showed that a trend toward increasing size persists with the addition of the more recently discovered mandibles, albeit with weakened statistical significance. The new LDD mandibles are consistent with a trend of increasing size: both LDD-VP-1/167 and

LDD-VP-1/672 come from older intervals and possess a small corpus.

Lockwood and colleagues further demonstrated that *A. afarensis* corpus size is significantly more variable than *Pan* and *Gorilla* comparative samples, but only if the entire hypodigm is considered (CV = 10.9, 3.5–3.0 Ma, $n = 20$). When the youngest interval was excluded, variation dropped to a level that no longer exceeded the magnitude seen in the comparative samples (CV = 8.36, 3.5–3.18 Ma, $n = 16$). Thus, the temporal trend (and time averaging of fossil samples) could account for the elevated variation. The expanded sample of *A. afarensis* mandibles (i.e., including DIK-2-1, MAK-VP-1/12, LDD-VP-1/167, and NFR-VP-1/29) achieves a similar magnitude of variation in a smaller, geographically constrained sample that spans an even shorter interval (CV = 8.44, ca. 3.5–3.3 Ma, $n = 12$).

Researchers have questioned whether previously identified temporal trends apply to the period covered by the lowest members of the Hadar Formation, and whether this older interval could exhibit more variation than later intervals (Alemseged et al., 2005). Our observations on the LDD sample confirm previous investigations into temporal trends, without markedly expanding the range of variation previously documented in *A. afarensis*. The value added with the LDD sample lies in its contribution to controlling for spatiotemporal differences among site samples. The addition of the LDD sample shows that a more tightly constrained spatiotemporal interval has the potential to retain most of the range of variation previously documented for some *A. afarensis* features. The sample size of hominin fossils older than 3.4 Ma within the Afar remains fairly small, but future work increasing this sample will help to differentiate the various factors that contribute to morphological variation.

4.3. Taxonomic diversity at Woranso-Mille

The discovery of the Burtele foot was the first evidence to suggest the presence of a non-*A. afarensis* hominin in the Afar Depression (Haile-Selassie et al., 2012). Since that time, dentognathic fossils from the Burtele area were attributed to the species *A. deyiremeda* (Haile-Selassie et al., 2015). The LDD hominin sample provides evidence for the presence of *A. afarensis* in strata contemporaneous with those at Burtele, thus the LDD specimens tighten the spatiotemporal parameters on the co-occurrence of the Burtele taxa and *A. afarensis*.

There is marginal evidence of taxonomic diversity in the LDD sample, based on the magnitude of variation in M_3 size (SOM S1 and SOM Fig. S6). The magnitude of variation present within the Woranso-Mille EEA M_3 sample ($n = 5$, ca.3.5–3.3 Ma) exceeds that present in *A. afarensis* or *A. africanus*, and this within a much more tightly confined spatiotemporal range. The LDD-VP-1/406 M_3 is similar to the *A. deyiremeda* holotype maxilla only in the very broadest sense of being dentally small. However, this similarity is insufficient to merit attribution to *A. deyiremeda*, especially given that the M_3 in the paratype mandible (BRT-VP-3/14) does not share the distinct morphology of LDD-VP-1/406. Although the LDD sample does not include any additional specimens attributable to *A. deyiremeda* nor any pedal elements that might be compared to BRT-VP-2/73, it provides potential support to a more general hypothesis that *A. afarensis* co-existed with at least one additional species at Woranso-Mille during the ca. 3.5–3.3 Ma period.

5. Conclusions

This article describes a new collection of hominin fossils from the LDD-VP-1 locality of Woranso-Mille. Most specimens in this sample exhibit diagnostic *A. afarensis* morphology, with particular affinity to the Hadar sample. These specimens increase *A. afarensis* sample size around 3.4 Ma, and morphology is generally consistent with previously documented levels of variation and temporal trends. Furthermore, the identification of *A. afarensis* at LDD provides the first conclusive evidence for the co-existence of *A. afarensis* and other non-*A. afarensis* species at Woranso-Mille during the 3.5–3.3 Ma time interval. We also describe an extremely small M_3 from LDD, similar to one recently reported from Lomekwi, Kenya. Although this LDD specimen may represent a developmental anomaly (i.e., M_4) or an idiosyncratically small individual, it may alternatively be attributable to a small-toothed, non-*A. afarensis* hominin.

Declaration of competing interest

The authors declare no competing interests.

Acknowledgments

Field and laboratory research was supported by the US National Science Foundation (BCS-1124705, BCS-1124713, BCS-1124716, BCS-1125157 and BCS-1125345), The Cleveland Museum of Natural History, the Leakey Foundation, and the National Geographic Society. Further laboratory work was supported by the Max Planck Institute for Evolutionary Anthropology. We thank the Authority for Research and Conservation of Cultural Heritage (ARCCH) for permission to conduct field and laboratory work in Ethiopia; the Afar people of Woranso-Mille and the Mille District administration for their hospitality and all crew members of the Woranso-Mille Paleontological Research Project. We also thank the following colleagues, curators, collections managers and institutions for access to specimens in their care: M. Endalamaw, Y. Assefa, T. Getachew, S. Melaku, G. Tekle and the National Museum of Ethiopia; F. Manthi and the National Museums of Kenya; A. Kwekason, the National Museum of Tanzania and the Tanzania Commission for Science and Technology; B. Zipfel and the Evolutionary Studies Institute and the University of Witwatersrand; H. Fourie, L. Kgasi and the Ditsong National Museum of Natural History; D. Lieberman and the Peabody Museum; M. Tocheri and the Smithsonian National Museum of Natural History; C. Funk and the Museum für Naturkunde; E. Gilissen and the Royal Museum for Central Africa; U. Schwarz and others contributing to the curation and digitalization of the MPI-EVA Tai Chimpanzee Collection and Tim Stecko at the Center for Quantitative Imaging, Pennsylvania State University. We are grateful to the following colleagues for their assistance in accessing collections, data sharing and discussions: T. Harrison, D. Su, W.H. Kimbel, T. White, G. Suwa, B. Asfaw, M. Skinner, F. Grine and J. Moggi-Cecchi.

Appendix A. Supplementary Online Material

Supplementary online material to this article can be found online at https://doi.org/10.1016/j.jhevol.2021.102956.

References

Alemseged, Z., Spoor, F., Kimbel, W.H., Bobe, R., Geraads, D., Reed, D., Wynn, J.G., 2006. A juvenile early hominin skeleton from Dikika, Ethiopia. Nature 443, 296–301.

Alemseged, Z., Wynn, J.G., Kimbel, W.H., Reed, D., Geraads, D., Bobe, R., 2005. A new hominin from the Basal Member of the Hadar Formation, Dikika, Ethiopia, and its geological context. J. Hum. Evol. 49, 499–514.

Alene, M., Hart, W.K., Saylor, B.Z., Deino, A., Mertzman, S., Haile-Selassie, Y., Gibert, L.B., 2017. Geochemistry of Woranso-Mille Pliocene basalts from west-central Afar, Ethiopia: Implications for mantle source characteristics and rift evolution. Lithos 282, 187–200.

Brown, F.H., 1982. Tulu Bor tuff at Koobi Fora correlated with the Sidi Hakoma tuff at Hadar. Nature 300, 631–633.
Brown, B., Brown, F.H., Walker, A., 2001. New hominids from the Lake Turkana basin, Kenya. J. Hum. Evol. 41, 29–44.
Brunet, M., Beauvilain, A., Coppens, Y., Heintz, E., Moutaye, A.H.E., Pilbeam, D., 1995. The first australopithecine 2,500 kilometres west of the Rift Valley (Chad). Nature 378, 273–275.
Brunet, M., Beauvilain, A., Coppens, Y., Heintz, E., Moutaye, A.H.E., Pilbeam, D., 1996. *Australopithecus bahrelghazali*, une nouvelle espèce d'Hominidé ancien de la région de Koro Toro (Tchad). C.R. Acad. Sci. Sér. 2. 322, 907–913.
Campisano, C.J., Feibel, C.S., 2008. Tephrostratigraphy of the Hadar and Busidima Formations at Hadar, Afar Depression, Ethiopia. In: Quade, J., Wynn, J.G. (Eds.), The Geology of Early Humans in the Horn of Africa. Geological Society of America, Boulder, pp. 135–162.
Coppens, Y., 1983. Systématique, phylogénie, environnement et culture des Australopithèques, hypothèses et synthèse. Bull. Mem. Soc. Anthropol. Paris 10, 273–284.
Deino, A.L., 2011. $^{40}Ar/^{39}Ar$ dating of Laetoli, Tanzania. In: Harrison, T. (Ed.), Paleontology and Geology of Laetoli: Human Evolution in Context. Volume 1: Geology, Geochronology, Paleoecology and Paleoenvironment. Springer, Dordrecht, pp. 77–97.
Deino, A.L., Scott, G.R., Saylor, B., Alene, M., Angelini, J.D., Haile-Selassie, Y., 2010. $^{40}Ar/^{39}Ar$ dating, paleomagnetism, and tephrochemistry of Pliocene strata of the hominid-bearing Woranso-Mille area, west-central Afar Rift, Ethiopia. J. Hum. Evol. 58, 111–126.
Delezene, L.K., Kimbel, W.H., 2011. Evolution of the mandibular third premolar crown in early *Australopithecus*. J. Hum. Evol. 60, 711–730.
deMenocal, P.B., Brown, F.H., 1999. Pliocene tephra correlations between East African hominid localities, the Gulf of Aden, and the Arabian Sea. In: Agusti, J., Rook, L., Andrews, P. (Eds.), Hominoid Evolution and Climatic Change in Europe, Volume 1. The Evolution of Neogene Terrestrial Ecosystems in Europe. Cambridge University Press, Cambridge, pp. 23–54.
Ditchfield, P., Harrison, T., 2011. Sedimentology, lithostratigraphy and depositional history of the Laetoli area. In: Harrison, T. (Ed.), Paleontology and Geology of Laetoli: Human Evolution in Context. Volume 1: Geology, Geochronology, Paleoecology and Paleoenvironment. Springer, Dordrecht, pp. 47–76.
Drapeau, M.S., Ward, C.V., Kimbel, W.H., Johanson, D.C., Rak, Y., 2005. Associated cranial and forelimb remains attributed to *Australopithecus afarensis* from Hadar, Ethiopia. J. Hum. Evol. 48, 593–642.
Gower, C.D., 1923. A contribution to the morphology of the apertura piriformis. Am. J. Phys. Anthropol. 6, 27–36.
Guy, F., Mackaye, H.T., Likius, A., Vignaud, P., Schmittbuhl, M., Brunet, M., 2008. Symphyseal shape variation in extant and fossil hominoids, and the symphysis of *Australopithecus bahrelghazali*. J. Hum. Evol. 55, 37–47.
Haile-Selassie, Y., 2010. Phylogeny of early *Australopithecus*: New fossil evidence from the Woranso-Mille (central Afar, Ethiopia). Philos. Trans. R. Soc. Lond. B Biol. Sci. 365, 3323–3331.
Haile-Selassie, Y., Gibert, L., Melillo, S.M., Ryan, T.M., Alene, M., Deino, A., Levin, N.E., Scott, G., Saylor, B.Z., 2015. New species from Ethiopia further expands Middle Pliocene hominin diversity. Nature 521, 483–488.
Haile-Selassie, Y., Latimer, B.M., Alene, M., Deino, A.L., Gibert, L., Melillo, S.M., Saylor, B.Z., Scott, G.R., Lovejoy, C.O., 2010a. An early *Australopithecus afarensis* postcranium from Woranso-Mille, Ethiopia. Proc. Natl. Acad. Sci. USA 107, 12121–12126.
Haile-Selassie, Y., Melillo, S.M., 2015. Middle Pliocene hominin mandibular fourth premolars from Woranso-Mille (Central Afar, Ethiopia). J. Hum. Evol. 78, 44–59.
Haile-Selassie, Y., Melillo, S.M., Ryan, T.M., Levin, N.E., Saylor, B.Z., Deino, A., Mundil, R., Scott, G., Mulugeta, A., Gibert, L., 2016a. Dentognathic remains of *Australopithecus afarensis* from Nefuraytu (Woranso-Mille, Ethiopia): Comparative description, geology, and paleoecological context. J. Hum. Evol. 100, 35–53.
Haile-Selassie, Y., Melillo, S.M., Su, D.F., 2016b. The Pliocene hominin diversity conundrum: Do more fossils mean less clarity? Proc. Natl. Acad. Sci. USA 113, 6364–6371.
Haile-Selassie, Y., Melillo, S.M., Vazzana, A., Benazzi, S., Ryan, T.M., 2019. A 3.8-million-year-old hominin cranium from Woranso-Mille, Ethiopia. Nature 573, 214–219.
Haile-Selassie, Y., Ryan, T.M., 2019. Comparative description and taxonomy of new hominin juvenile mandibles from the Pliocene of Woranso-Mille (Central Afar, Ethiopia). J. Hum. Evol. 132, 15–31.
Haile-Selassie, Y., Saylor, B.Z., Deino, A., Alene, M., Latimer, B.M., 2010b. New hominid fossils from Woranso-Mille (Central Afar, Ethiopia) and taxonomy of early *Australopithecus*. Am. J. Phys. Anthropol. 141, 406–417.
Haile-Selassie, Y., Saylor, B.Z., Deino, A., Levin, N.E., Alene, M., Latimer, B.M., 2012. A new hominin foot from Ethiopia shows multiple Pliocene bipedal adaptations. Nature 483, 565–569.
Harrison, T., 2011. Hominins from the Upper Laetolil and Upper Ndolanya Beds, Laetoli. In: Harrison, T. (Ed.), Paleontology and Geology of Laetoli: Human Evolution in Context. Volume 2: Fossil Hominins and the Associated Fauna. Springer, Dordrecht, pp. 141–188.
Hlusko, L.J., 2004. Protostylid variation in *Australopithecus*. J. Hum. Evol. 46, 579–594.
Johanson, D.C., Lovejoy, C.O., Kimbel, W.H., White, T.D., Ward, S.C., Bush, M.E., Latimer, B.M., Coppens, Y., 1982a. Morphology of the Pliocene partial hominid skeleton (AL 288-1) from the Hadar formation, Ethiopia. Am. J. Phys. Anthropol. 57, 403–451.
Johanson, D.C., White, T.D., 1979. A systematic assessment of early African hominids. Science 203, 321–330.
Johanson, D.C., White, T.D., Coppens, Y., 1978. A new species of the genus *Australopithecus* (Primates: Hominidae) from the Pliocene of Eastern Africa. Kirtlandia 28, 1–14.
Johanson, D.C., White, T.D., Coppens, Y., 1982b. Dental remains from the Hadar Formation, Ethiopia: 1974–1977 collections. Am. J. Phys. Anthropol. 57, 545–603.
Kimbel, W.H., 2015. The Species and Diversity of Australopiths. In: Henke, W., Tattersall, I. (Eds.), Handbook of Paleoanthropology. Springer, Berlin, pp. 2071–2105.
Kimbel, W.H., Delezene, L.K., 2009. "Lucy" redux: A review of research on *Australopithecus afarensis*. Am. J. Phys. Anthropol. 140, 2–48.
Kimbel, W.H., Johanson, D.C., Coppens, Y., 1982. Pliocene hominid cranial remains from the Hadar Formation, Ethiopia. Am. J. Phys. Anthropol. 57, 453–499.
Kimbel, W.H., Lockwood, C.A., Ward, C.V., Leakey, M.G., Rak, Y., Johanson, D.C., 2006. Was *Australopithecus anamensis* ancestral to *A. afarensis*? A case of anagenesis in the hominin fossil record. J. Hum. Evol. 51, 134–152.
Kimbel, W.H., Rak, Y., 2010. The cranial base of *Australopithecus afarensis*: New insights from the female skull. Philos. Trans. R. Soc. Lond. B Biol. Sci. 365, 3365–3376.
Kimbel, W.H., Rak, Y., Johanson, D.C., 2004. The Skull of *Australopithecus afarensis*. Oxford Univeristy Press, Oxford.
Kimbel, W.H., White, T.D., Johanson, D.C., 1985. Craniodental morphology of the hominids from Hadar and Laetoli: Evidence of "*Paranthropus*"and *Homo* in the mid-Piocene of eastern Africa? In: Delson, E. (Ed.), Ancestors: The Hard Evidence. Alan R. Liss, New York, pp. 120–137.
Kirschvink, J.L., 1980. The least-squares line and plane and the analysis of palaeomagnetic data. Geophys. J. Int. 62, 699–718.
Klein, R.G., 2016. Issues in human evolution. Proc. Natl. Acad. Sci. USA 113, 6345–6347.
Leakey, M.G., Feibel, C.S., McDougall, I., Walker, A., 1995. New four-million-year-old hominid species from Kanapoi and Allia Bay, Kenya. Nature 376, 565–571.
Leakey, M.G., Spoor, F., Brown, F.H., Gathogo, P.N., Kiarie, C., Leakey, L.N., McDougall, I., 2001. New hominin genus from eastern Africa shows diverse middle Pliocene lineages. Nature 410, 433–440.
Lockwood, C.A., Kimbel, W.H., Johanson, D.C., 2000. Temporal trends and metric variation in the mandibles and dentition of *Australopithecus afarensis*. J. Hum. Evol. 39, 23–55.
Lockwood, C.A., Tobias, P.V., 1999. A large male hominin cranium from Sterkfontein, South Africa, and the status of *Australopithecus africanus*. J. Hum. Evol. 36, 637–685.
Lovejoy, C.O., Meindl, R.S., Ohman, J.C., Heiple, K.G., White, T.D., 2002. The Maka femur and its bearing on the antiquity of human walking: Applying contemporary concepts of morphogenesis to the human fossil record. Am. J. Phys. Anthropol. 119, 97–133.
Manthi, F.K., Plavcan, J.M., Ward, C.V., 2012. New hominin fossils from Kanapoi, Kenya, and the mosaic evolution of canine teeth in early hominins. South Afr. J. Sci. 108, 1–9.
Mbua, E., Kusaka, S., Kunimatsu, Y., Geraads, D., Sawada, Y., Brown, F.H., Sakai, T., Boisserie, J.R., Saneyoshi, M., Omuombo, C., Muteti, S., Hirata, T., Hayashida, A., Iwano, H., Danhara, T., Bobe, R., Jicha, B., Nakatsukasa, M., 2016. Kantis: A new *Australopithecus* site on the shoulders of the Rift Valley near Nairobi, Kenya. J. Hum. Evol. 94, 28–44.
McCollum, M.A., 2000. Subnasal morphological variation in fossil hominids: A reassessment based on new observations and recent developmental findings. Am. J. Phys. Anthropol. 112, 275–283.
McCollum, M.A., Grine, F.E., Ward, S.C., Kimbel, W.H., 1993. Subnasal morphological variation in extant hominoids and fossil hominids. J. Hum. Evol. 24, 87–111.
Moggi-Cecchi, J., Grine, F.E., Tobias, P.V., 2006. Early hominid dental remains from Members 4 and 5 of the Sterkfontein Formation (1966–1996 excavations): Catalogue, individual associations, morphological descriptions and initial metrical analysis. J. Hum. Evol. 50, 239–328.
Moore, N.C., Thackeray, J.F., Hublin, J.-J., Skinner, M.M., 2016. Premolar root and canal variation in South African Plio-Pleistocene specimens attributed to *Australopithecus africanus* and *Paranthropus robustus*. J. Hum. Evol. 93, 46–62.
Olson, T.R., 1981. Basicranial morphology of the extant hominoids and Pliocene hominids: The new material from the Hadar Formation, Ethiopia and its significance in early human evolution and taxonomy. In: Stringer, C.B. (Ed.), Aspects of Human Evolution. Taylor and Francis, London, pp. 99–128.
Olson, T.R., 1985. Cranial morphology and systematics of the Hadar Formation hominids and "*Australopithecus*" *africanus*. In: Delson, E. (Ed.), Ancestors: The Hard Evidence. Alan R. Liss, New York, pp. 102–119.
Plavcan, J.M., Lockwood, C.A., Kimbel, W.H., Lague, M.R., Harmon, E.H., 2005. Sexual dimorphism in *Australopithecus afarensis* revisited: How strong is the case for a human-like pattern of dimorphism? J. Hum. Evol. 48, 313–320.
Puech, P.-F., Cianfarani, F., Roth, H., 1986. Reconstruction of the maxillary dental arcade of Garusi Hominid 1. J. Hum. Evol. 15, 325–332.
Remane, A., 1954. Structure and relationships of *Meganthropus africanus*. Am. J. Phys. Anthropol. 12, 123–126.
Reno, P.L., Lovejoy, C.O., 2015. From Lucy to Kadanuumuu: Balanced analyses of *Australopithecus afarensis* assemblages confirm only moderate skeletal dimorphism. PeerJ 3, e925.

Reno, P.L., McCollum, M.A., Meindl, R.S., Lovejoy, C.O., 2010. An enlarged postcranial sample confirms *Australopithecus afarensis* dimorphism was similar to modern humans. Philos. Trans. R. Soc. Lond. B Biol. Sci. 365, 3355–3363.
Sarna-Wojcicki, A.M., Meyer, C.E., Roth, P.H., Brown, F.H., 1985. Ages of tuff beds at East African early hominid sites and sediments in the Gulf of Aden. Nature 313, 306–308.
Saylor, B.Z., Angelini, J., Deino, A., Alene, M., Fournelle, J.H., Haile-Selassie, Y., 2016. Tephrostratigraphy of the Waki-Mille area of the Woranso-Mille paleoanthropological research project, Afar, Ethiopia. J. Hum. Evol. 93, 25–45.
Saylor, B.Z., Gibert, L., Deino, A., Alene, M., Levin, N.E., Melillo, S.M., Peaple, M.D., Feakins, S.J., Bourel, B., Barboni, D., Novello, A., Sylvestre, F., Mertzman, S.A., Haile-Selassie, Y., 2019. Age and context of mid-Pliocene hominin cranium from Woranso-Mille, Ethiopia. Nature 573, 220–224.
Schwartz, J.H., 1984. Supernumerary teeth in anthropoid primates and models of tooth development. Arch. Oral Biol. 29, 833–842.
Sénut, B., 1983. Les hominides Plio-Pleistocenes: essai taxinomique et phylogenetique a partir de certains os longs. Bull. Mem. Soc. Anthropol. Paris 10, 325–334.
Senut, B., Tardieu, C., 1985. Functional aspects of Plio-Pleistocene hominid limb bones: Implications for taxonomy and phylogeny. In: Delson, E. (Ed.), Ancestors: The Hard Evidence. Alan R. Liss, New York, pp. 193–201.
Şenyürek, M., 1955. A note on the teeth of *Meganthropus africanus* Weinert from Tanganyika Territory. Belleten 19, 1–55.
Skinner, M.M., Wood, B.A., Boesch, C., Olejniczak, A.J., Rosas, A., Smith, T.M., Hublin, J.-J., 2008. Dental trait expression at the enamel-dentine junction of lower molars in extant and fossil hominoids. J. Hum. Evol. 54, 173–186.
Skinner, M.M., Alemseged, Z., Gaunitz, C., Hublin, J.J., 2015. Enamel thickness trends in Plio-Pleistocene hominin mandibular molars. J. Hum. Evol. 85, 35–45.
Skinner, M.M., Leakey, M.G., Leakey, L.N., Manthi, F.K., Spoor, F., 2020. Hominin dental remains from the Pliocene localities at Lomekwi, Kenya (1982–2009). J. Hum. Evol. 145, 102820 https://doi.org/10.1016/j.jhevol.2020.102820.
Spoor, F., Leakey, M.G., Leakey, L.N., 2010. Hominin diversity in the Middle Pliocene of eastern Africa: The maxilla of KNM-WT 40000. Philos. Trans. R. Soc. Lond. B Biol. Sci. 365, 3377–3388.
Spoor, F., Leakey, M.G., O'Higgins, P., 2016. Middle Pliocene hominin diversity: *Australopithecus deyiremeda* and *Kenyanthropus platyops*. Philos. Trans. R. Soc. Lond. B Biol. Sci. 371, 20150231.
Suwa, G., 1990. A comparative analysis of hominid dental remains from the Shungura and Usno Formations, Omo valley, Ethiopia. Ph.D. Dissertation, University of California, Berkeley.
Suwa, G., Wood, B.A., White, T.D., 1994. Further analysis of mandibular molar crown and cusp areas in Pliocene and early Pleistocene hominids. Am. J. Phys. Anthropol. 93, 407–426.
Walter, R.C., Aronson, J.L., 1993. Age and source of the Sidi Hakoma tuff, Hadar formation, Ethiopia. J. Hum. Evol. 25, 229–240.
Ward, C.V., Leakey, M.G., Walker, A., 1999. The New Hominid Species *Australopithecus anamensis*. Evol. Anthropol. 7, 197–205.
Ward, C.V., Leakey, M.G., Walker, A., 2001. Morphology of *Australopithecus anamensis* from Kanapoi and Allia Bay, Kenya. J. Hum. Evol. 41, 255–368.
Ward, C.V., Manthi, F.K., Plavcan, J.M., 2013. New fossils of *Australopithecus anamensis* from Kanapoi, West Turkana, Kenya (2003–2008). J. Hum. Evol. 65, 501–524.
Ward, C.V., Plavcan, J.M., Manthi, F.K., 2020. New fossils of *Australopithecus anamensis* from Kanapoi, West Turkana, Kenya (2012–2015). J. Hum. Evol. 140, 102368.
White, T.D., 1977. New fossil hominids from Laetolil, Tanzania. Am. J. Phys. Anthropol. 46, 197–229.
White, T.D., 1980. Additional fossil hominids from Laetoli, Tanzania: 1976–1979 specimens. Am. J. Phys. Anthropol. 53, 487–504.
White, T.D., 1985. The hominids of Hadar and Laetoli: An element-by-element comparison of the dental samples. In: Delson, E. (Ed.), Ancestors: The Hard Evidence. Alan R. Liss, New York, pp. 138–152.
White, T.D., Johanson, D.C., 1982. Pliocene hominid mandibles from the Hadar Formation, Ethiopia: 1974–1977 collections. Am. J. Phys. Anthropol. 57, 501–544.
White, T.D., Johanson, D.C., Kimbel, W.H., 1983. *Australopithecus africanus*, its phyletic position reconsidered. In: Ciochon, R.L., Corruccini, R.S. (Eds.), New Interpretations of Ape and Human Ancestry. Plenum Press, New York, pp. 721–780.
White, T.D., Suwa, G., Hart, W.K., Walter, R.C., WoldeGabriel, G., de Heinzelin, J., Clark, J.D., Asfaw, B., Vrba, E.S., 1993. New discoveries of *Australopithecus* at Maka in Ethiopia. Nature 366, 261–265.
White, T.D., Suwa, G., Simpson, S.W., Asfaw, B., 2000. Jaws and teeth of *Australopithecus afarensis* from Maka, Middle Awash, Ethiopia. Am. J. Phys. Anthropol. 111, 45–68.
WoldeGabriel, G., Endale, T., White, T.D., Thouveny, N., Hart, W.K., Renne, P.R., Asfaw, B., 2013. The role of tephra studies in African paleoanthropology as exemplified by the Sidi Hakoma Tuff. J. Afr. Earth Sci. 77, 41–58.
Wood, B., Abbott, S.A., 1983. Analysis of the dental morphology of Plio-Pleistocene hominids. I. Mandibular molars: Crown area measurements and morphological traits. J. Anat. 136, 197–219.
Wood, B., Abbott, S.A., Graham, S.H., 1983. Analysis of the dental morphology of Plio-Pleistocene homininds. II. Mandibular molars—study of cusp areas, fissure pattern and cross sectional shape of the crown. J. Anat. 137, 287–314.
Wood, B., Boyle, E.K., 2016. Hominin taxic diversity: Fact or fantasy? Yearbk. Phys. Anthropol. 159, S37–S78.
Wood, B., Engleman, C., 1988. Analysis of the dental morphology of Plio-Pleistocene hominids. V. Maxillary postcanine tooth morphology. J. Anat. 161, 1–35.
Wood, B., Uytterschaut, H., 1987. Analysis of the dental morphology of Plio-Pleistocene homininds. III. Mandibular premolar crowns. J. Anat. 154, 121–156.